EUMETSAT

MTG-FCI: ATBD for Optimal Cloud Analysis Product

Doc.No. : EUM/MTG/DOC/11/0654
Issue : v5 e-signed
Date : 1 September 2016
WBS : MTG-834200

EUMETSAT
Eumetsat-Allee 1, D-64295 Darmstadt, Germany
Tel: +49 6151 807-7
Fax: +49 6151 807 555
http://www.eumetsat.int

Page left intentionally blank

Document Change Record

Issue / Revision	*Remarks*
v1 Draft	For internal review
v1 of 31 January 2011	First published version
v3B of 24 October 2011	Second published version following the recommendations of the System PDR Science Panel
v4 of 15 January 2013	Updated to include 2-layer cloud detection and retrieval; more comprehensive details on first guess procedures; other pertinent details that became apparent with the developments of the L2PGS Doc. Note section 5 Product Characteristics should be updated to include characteristics including 2-layer results although a full description is available through the peer-reviewed publication RD-3.
v5 of 01 September 2016 (MTG_DCR_154)	Updated to include functionality to retrieve cloud properties based on input flag from an external (scenes analysis) source indicating volcanic ash and mineral dust.

Table of Contents

1 Introduction 6
1.1 Purpose of this Document 6
1.2 Structure of this Document 6
1.3 Applicable and Reference Documents 6
1.4 Acronyms and Definitions 7
2 Overview 8
2.1 Relevant Instrument Characteristics 8
2.2 Generated Products 10
3 Algorithm Description 11
3.1 Physical Basis Overview 11
3.2 Assumptions and Limitations 14
3.3 Algorithm Basis Overview 15
3.4 Algorithm Input 18
3.4.1 Primary Sensor Data 18
3.4.2 Ancillary Dynamic Data 19
3.4.2.1 Imagery: Cloud Mask 19
3.4.2.2 NWP: Atmospheric Profiles and RT Quantities 19
3.4.3 Ancillary Static Data 21
3.4.3.1 Static Pixel Based Ancillary Data 21
3.4.3.2 Cloud Radiative Property LUTs 21
3.5 Detailed Description 23
3.5.1 Physical Description 23
3.5.1.1 The Cloud State Parameters, x 23
3.5.1.2 The Measurements, y 25
3.5.1.3 The Atmospheric Model Parameters, b 26
3.5.1.4 Fast Forward Model: Solar 26
3.5.1.5 Fast Forward Model: Thermal 27
3.5.1.6 Cost Function 27
3.5.1.7 Minimising the cost function 28
3.5.2 Mathematical Description 31
3.5.2.1 Radiative Transfer 31
3.5.2.1.1 Solar Forward Model 31
3.5.2.1.2 Solar Jacobian Model 32
3.5.2.1.3 Thermal Forward Model 33
3.5.2.1.4 Thermal Jacobian Model 34
3.5.2.2 Cost Function and Minimisation 35
3.5.2.3 Output parameters 36
3.5.2.4 Error Analysis 37
3.5.3 Operational Considerations 40
3.6 Output Description 40
4 Implications of new FCI channels and characteristics 42
4.1 Additional Channels 42
4.1.1 2.2 micron 42
4.1.2 0.96 micron 42
4.1.3 1.38 micron 42
4.1.4 0.44, 0.5 microns 42
4.2 Altered Channels 43
4.2.1 0.86 micron 43
4.2.2 1.61 micron 43
4.2.3 3.8 micron 43
4.3 High Spatial Resolution 43
4.4 IRS sounder 44
5 Product Characteristics 45
5.1 Diagnostics: Measurement Cost, Iterations and Residuals 45

5.2 Cloud Phase 47
5.3 COT 48
5.4 CRE 48
5.5 CTP 49
6 Product Validation 51
6.1 COT compared to MODIS 51
6.2 CRE compared to MODIS 51
6.3 LWP compared to AMSR 52
6.4 CTP compared to CPR and CALIOP 53
6.4.1 Accuracy and QC measures 53
6.4.2 Multi-layer cloud 55
6.4.3 Boundary layer temperature inversions 57
7 Future Developments 60
7.1 Improved treatment of Multi-Layer Cloud 60
7.2 Imagery based ancillary data 60
8 APPENDIX: Identification and Modification of Profile Temperature Inversions 61
8.1 Tropopause 61
8.2 Boundary Layer Inversions 62
9 APPENDIX: Inversion First Guess procedures 64
9.1 First Guess Cloud Phase, CPH_{FG} 64
9.2 First Guess Optical Thickness, COT_{FG} 65
9.3 First Guess Effective Radius, CRE_{FG} 66
9.4 First Guess Cloud Top Pressure, CTP_{FG} 66
9.5 Control and first guess parameters for the Two Layer model 67
APPENDIX: Functional Details of marquardt inversion 68
9.6 Calc: y, K(x) 68
9.7 Set: S_y 68
9.8 Calc J(x) 69
9.9 Set Marquardt parameter 69
9.10 Calc δx 69
9.11 Bounds check 69
9.12 Phase change 70
9.13 Set α 70
9.14 Convergence test 70
9.15 Test 2-Layer 71
9.16 Initialise 2-Layer 71
9.17 Save SL result 71
10 APPENDIX: Model Selection and Extraction of 2-Layer Parameters 72
10.1 Model selection 72
10.2 2-Layer product and error extraction 72
11 APPENDIX: Gradient model workings 75
12 Glossary 76
13 Constants 78

1 INTRODUCTION

1.1 Purpose of this Document

This document describes the algorithm theoretical basis of the Optimal Cloud Analysis (OCA) product, as it shall be derived from the Meteosat Third Generation Flexible Combined Imager (MTG-FCI). It supplies additionally some validation results.

1.2 Structure of this Document

Section 2 of this document provides a short overview over the MTG imaging instrument characteristics and the derived meteorological products, which will be referenced later in the text. This is followed by a detailed description of the underlying algorithm of the OCA product. Section 3 is structured in an order of generally increasing detail on the principles and theory behind OCA. Section 4 addresses the consequences of additional and altered channel characteristics that arise with OCA applied to the FCI instead of the SEVIRI instrument upon which all the current experience lies. As an aid to successful implementation and anomaly spotting, section 5 demonstrates typical characteristics of the algorithm output. Both product and quality control information characteristics are described. Section 6 provides some insight into product quality using validation made with A-Train sensor data. Section 7 describes future developments that currently appear to be likely. A number of Appendices provide details of algorithm operations.
A full list of acronyms is provided in section 1.4, literature references are listed in section 8, section 9 provides a detailed analysis of the OCA radiative transfer model gradient and section 12 provides a glossary of mathematical terms used.

1.3 Applicable and Reference Documents

The following documents have been used to establish this document:

Doc ID	*Title*	*Reference*
[AD-1]	MTG End Users Requirements Document	EUM/MTG/SPE/07/0036
[AD-2]	MTG Products in the Level-2 Processing Facility	EUM/C/70/10/DOC/08
[AD-3]	Radiative Transfer Model within the FCI Level 2 Processing	EUM/MTG/DOC/10/0382
[RD-1]	OCA research study report	Watts et al. Study Report 1998 *ITT 97/181, Rutherford Appleton Laboratory*
[RD-2]	OCA cloud model study report	Siddans et al. Study Report 2010, *EUM/CO/07/4600000463/ PDW. Rutherford Appleton Laboratory*

[RD-3]	OCA 2-Layer application and validation	Watts et al, *J. Geophys. Res., 116, D16203, doi:10.1029/*

1.4 Acronyms and Definitions

The following table lists definitions for all acronyms used in this document.

Acronym	*Full Name*
AMSR-E	Advanced Microwave Scanning Radiometer-EOS
CRM	Clear Sky Reflectance Map
CALIOP	Cloud-Aerosol Lidar with Orthogonal Polarization
CPR	Cloud Profiling Radar
FCI	Flexible Combined Imager
FCI-FDSS	FCI Full Disk Scanning Service
FCI-RSS	FCI Rapid Scanning Service
FDHSI	Full Disk High Spectral Resolution Imagery
HRFI	High Spatial Resolution Fast Imagery
HRV	High Resolution Visible Channel of SEVIRI
IR	Infrared
MODIS	Moderate-resolution Imaging Spectroradiometer
MSG	Meteosat Second Generation
MTG	Meteosat Third Generation
NIR	Near Infrared
NWP	Numerical Weather Prediction
OCA	Optimal Cloud Analysis
RTM	Radiative Transfer Model
RTTOV	Radiative Transfer for TOVS
SCE	Scene Identification
SEVIRI	Spinning Enhanced Visible and Infrared Imager
SSD	Spatial Sampling Distance
VIS	Visible (solar)
COT	Cloud Optical Thickness (as retrieved parameter)
CRE	Cloud Effective Radius (“)
CTP	Cloud Top Pressure (“)
CFR	Cloud Fraction (“)
CPHS	Cloud Phase (“)
TS	Skin (surface) Temperature (“)

2 OVERVIEW

2.1 Relevant Instrument Characteristics

The mission of the Meteosat Third Generation (MTG) System is to provide continuous high spatial, spectral and temporal resolution observations and geophysical parameters of the Earth / Atmosphere System derived from direct measurements of its emitted and reflected radiation using satellite based sensors from the geo-stationary orbit to continue and enhance the services offered by the Second Generation of the Meteosat System (MSG) and its main instrument SEVIRI.

The meteorological products described in this document will be extracted from the data of the Flexible Combined Imager (FCI) mission. The FCI is able to scan either the full disk in 16 channels every 10 minutes with a spatial sampling distance in the range 1 – 2 km (Full Disk High Spectral Resolution Imagery (FDHSI) in support of the Full Disk Scanning Service (FCI-FDSS)) or a quarter of the earth in 4 channels every 2.5 minutes with doubled resolution (High spatial Resolution Fast Imagery (HRFI) in support of the Rapid Scanning Service (FCI-RSS)).

FDHSI and HRFI scanning can be interleaved on a single satellite (e.g. when only one imaging satellite is operational in orbit) or conducted in parallel when 2 satellites are available in orbit. Table 1 provides an overview over the FCI spectral channels and their respective spatial resolution.

The FCI acquires the spectral channels simultaneously by scanning a detector array per spectral channel in an east/west direction to form a swath. The swaths are collected moving from south to north to form an image per spectral channel covering either the full disc coverage or the local area coverage within the respective repeat cycle duration. Radiance samples are created from the detector elements at specific spatial sample locations and are then rectified to a reference grid, before dissemination to the End Users as Level 1 datasets. Spectral channels may be sampled at more than one spatial sampling distance or radiometric resolution, where the spectral channel has to fulfil FDHSI and HRFI missions or present data over an extended radiometric measurement range for fire detection applications.

***Table 1*: Channel specification for the Flexible Combined Imager (FCI)**

Spectral Channel	*Central Wavelength, $\lambda 0$*	*Spectral Width, $\Delta\lambda 0$*	*Spatial Sampling Distance (SSD)*
VIS 0.4	0.444 µm	0.060 µm	1.0 km
VIS 0.5	0.510 µm	0.040 µm	1.0 km
VIS 0.6	0.640 µm	0.050 µm	1.0 km 0.5 km [#1]
VIS 0.8	0.865 µm	0.050 µm	1.0 km
VIS 0.9	0.914 µm	0.020 µm	1.0 km
NIR 1.3	1.380 µm	0.030 µm	1.0 km
NIR 1.6	1.610 µm	0.050 µm	1.0 km
NIR 2.2	2.250 µm	0.050 µm	1.0 km 0.5 km [#1]
IR 3.8 (TIR)	3.800 µm	0.400 µm	2.0 km 1.0 km [#1]
WV 6.3	6.300 µm	1.000 µm	2.0 km
WV 7.3	7.350 µm	0.500 µm	2.0 km
IR 8.7 (TIR)	8.700 µm	0.400 µm	2.0 km
IR 9.7 (O_3)	9.660 µm	0.300 µm	2.0 km
IR 10.5 (TIR)	10.500 µm	0.700 µm	2.0 km 1.0 km [#1]
IR 12.3 (TIR)	12.300 µm	0.500 µm	2.0 km
IR 13.3 (CO_2)	13.300 µm	0.600 µm	2.0 km

[#1]: The spectral channels VIS 0.6, NIR 2.2, IR 3.8 and IR 10.5 are delivered in both FDHSI sampling and a HRFI sampling configurations.

2.2 Generated Products

The agreed list of MTG-FCI Level 2 products is detailed in [AD-2] and is repeated here for easy reference:

1. **SCE-CLA**:
   Scene Identification (cloudy, cloud free, dust, volcanic ash, fire) and a number of cloud products (cloud top height, phase)
2. **OCA**:
   Cloud Product (cloud top height and temperature, cloud top phase (liquid, ice, dust or volcanic ash), cloud top effective particle size, cloud optical depth, cloud sub-pixel fraction)
3. **ASR**:
   All Sky Radiance (mean IR radiance on an n x n pixel grid, together with other statistical information, for different scenes)
4. **CRM**:
   Clear Sky Reflectance Map (VIS reflectance for all non-absorbing channels, accumulated over time)
5. **GII**:
   Global Instability Indices (a number of atmospheric instability indices and layer precipitable water contents)
6. **TOZ**:
   Total Column Ozone
7. **AER**:
   Aerosol Product (asymmetry parameter, total column aerosol optical depth, refractive index, single scattering albedo, size distribution)
8. **AMV**:
   Atmospheric Motion Vectors (vector describing the displacement of clouds or water vapour features over three consecutive images, together with a vector height)
9. **OLR**:
   Outgoing Longwave Radiation (thermal radiation flux at the top of the atmosphere leaving the earth-atmosphere system)

The products will be derived from the spectral channel information provided by the FDHSI mission, on the resolution detailed in [AD-2].

An important tool for product extraction is a radiative transfer model (RTM), as described in [AD-3]. The IR model choice for the Level 2 product extraction is RTTOV, which is developed and maintained by the Satellite Application Facility on Numerical Weather Prediction (NWP-SAF). An RTM for solar channels is likely to be product specific and yet to be fully determined.

This ATBD describes the algorithm of the OCA product. The retrieval process makes use of the results of the SCE product.

3 ALGORITHM DESCRIPTION

OCA - 'Optimal Cloud Algorithm' - was so named to describe the approach taken to estimation of cloud properties from the MSG SEVIRI instrument, for which it was originally developed. The approach justifies the description 'optimal' from two of its characteristics; firstly that all measurements and all important cloud parameters are dealt with **simultaneously** and secondly that the formal technique of **optimal estimation** (OE) is employed to obtain a solution. The simultaneity characteristic aims to ensure that all information in a measurement is effectively extracted; the corollary of which is that all effects on a measurement are modelled. The OE framework aims to ensure that measurements and any prior information may be given appropriate weight in the solution depending on error characteristics whether instrumental or from modelling sources.

3.1 Physical Basis Overview

The FCI measurements distributed throughout the spectrum from 0.4 to 13.3 μm respond in a variety of ways to atmospheric and cloud conditions[1]. Apart from the strongly absorbing water vapour channels (at 1.3 and 6.3 μm) and low cloud situations, all channels will record a measurable response to the presence of cloud.

Shortwave (VIS) radiation in the range 0.4 - 0.9 μm is more or less conservatively scattered - that is to say there is effectively no absorption by the cloud particles, there is only scattering. These channels therefore respond primarily to the total cloud optical depth[2]. The scattering effectiveness is however affected to a small degree by particle size and shape, and the measurements include, depending on cloud thickness, reflection from the underlying physical surface. Absorption and scattering by atmospheric gases and aerosols vary considerably by location, view and solar geometries, and these effects have to be taken into account when interpreting the VIS measurements.

In the Near-infrared (NIR) at 1.6 and 2.2 μm, cloud liquid and ice water absorbs radiation to varying degrees but there is no significant emission. The absorption takes place whilst the radiation passes through the particle and the larger the particle the greater the absorption. The cloud reflectance in these channels is therefore responsive not only to cloud thickness but to the characteristic size (and shape) of the particles within the cloud. The exact distribution of the particles sizes is of secondary importance and a single 'effective radius' is used to characterize the particle size.

Size dependent particle absorption similarly takes place at the TIR 3.8 μm channel wavelength; the principle difference to the NIR channels is that at 3.8 μm there is significant

[1] The term 'cloud' is in the vast majority of cases meant to imply 'meteorological' i.e. liquid (water) and solid (ice) clouds. However, the OCA algorithm also retrieves dust and volcanic ash cloud properties when this is flagged on input from the SCE/CLA product. There is no conceptual or actual algorithmic difference in the treatment of ash clouds in the retrieval process – all physical properties are encapsulated in the radiative property lookup tables (LUTs).

[2] Ash particles absorb in these wavelengths.

thermal emission which must be modelled; the cloud emissivity is similarly particle size dependent.
There is some concern that there are significant effects of the size distribution width (normally expressed in terms of the 'effective variance') and the effective penetration depth into the cloud. This would mean that the use of all three absorption channels (1.6, 2.2 and 3.8 micron) will require the cloud model to somehow represent these properties; currently this is not the case.

The particle absorption at 3.8 μm and particularly 1.6 μm depends on the cloud phase with, in the 1.6 μm case, greater absorption when the cloud particles are in ice phase. Reflectance of solar irradiation by ice clouds is therefore lower for ice clouds than water clouds of a given optical depth and particle size[3].

For the channels that lie in the thermal infrared (TIR) the cloud temperature or altitude is the principal determining factor in the radiances measured. Many clouds however, particularly cirrus, are optically thin and so radiance transmitted from the atmosphere below makes a significant contribution to the overall signal; the interplay between cloud temperature and optical depth is therefore an important aspect. All the TIR channels are affected to a greater or lesser degree by atmospheric gas absorption and emission and this must be modelled. Were the atmospheric temperature always to be monotonically decreasing (with altitude) and the clouds always present in opaque overcast single layers, atmospheric absorption in the TIR would be mostly an irritating factor to be minimised. Given the real nature of the clouds and atmosphere, differential absorption of the TIR channels is a benefit as it allows for the discrimination of the various effects. The 13.3 μm channel is present, for example, because with well characterised CO_2 absorption it has a different sensitivity to cloud altitude and amount than a more transparent channel like the 10.5 μm. Other TIR channels like the water vapour sensitive 6.3 and 7.3 μm can aid in this discrimination despite the uncertainty in their modelling caused by uncertainties in the atmospheric water vapour concentrations. OCA capitalises on these differential absorptions in a way other than pure property estimation - its aim to fit all channel measurements with a single set of cloud model parameters enables a natural detection of cases where the cloud model does not apply (e.g. multi-layer cloud).

All channels are sensitive to the pixel cloud fraction. The sensitivities are similar in the channels groups; for example, the VIS channels are all similarly sensitive over dark (ocean) surfaces. Over land where the surface reflectance varies spectrally, the sensitivities can be different. In the TIR the sensitivity of 8.7, 10.5 and 12.3 μm are expected to be similar, again where the underlying surface is spectrally neutral. Despite this range of sensitivities, the overall estimation process is challenging and to date, for MSG SEVIRI, the cloud fraction parameter is essentially not estimated (it is assumed to be unity). This is not because the fraction is necessarily any harder to estimate than altitude or optical depth, but because its actual distribution in nature for a pixel size of ~2-5 Km is far from uniform. Most pixels will be found to be essentially fully cloudy (fraction = 1) or fully clear, whereas distributions of optical depth and altitude are more uniform. It is expected that with eventual more accurate specification of auxiliary information (e.g. surface reflectance, temperature etc) and greater constraints with more channels on the FCI, the pixel fraction will become estimable along with the other parameters.

[3] Ash has different properties at these wavelengths.

Table 2 gives a *qualitative* indication of the responses in the FCI channels to the main cloud parameters. It is important to note that the strength of response can be very dependent on the actual cloud conditions and in some cases on other factors such as viewing and solar geometry.

***Table 2*: Indicative channel responses to cloud parameters**

	Optical thickness COT	Effective radius CRE	Pressure (top) CTP	Fraction CFR	Phase CPHS	Skin T TS	Notes..
VIS 0.4	Strong	weak	weak[1]	moderate	weak	none	[1]Rayleigh effects may be important
VIS 0.5	Strong	weak	weak[1]	moderate	weak	none	[1]Rayleigh effects may be important
VIS 0.6	Strong	weak		strong	weak	none	
VIS 0.8	Strong	weak		strong	weak	none	
VIS 0.9	strong[1]	weak	strong	moderate	weak	none	[1]Depending on water vapour loading
NIR 1.3	moderate[1]	weak	strong[1]	moderate	weak	none	[1]Depending on cloud altitude
NIR 1.6	moderate[1]	strong	weak	strong	strong	none	[1]Saturates at high COT
NIR 2.2	moderate[1]	strong	weak	strong	moderate	none	[1]Saturates at high COT
IR 3.8 (TIR)	weak[1]	strong	strong	strong	moderate	strong	[1]Saturates at moderate COT
WV 6.3	Weak	weak	strong[1]	strong[1]	weak	none	[1]only for high clouds
WV 7.3	Weak	weak	strong[1]	strong[1]	weak	weak	[1]only for medium and high clouds
IR 8.7 (TIR)	weak[1]	weak	strong	strong	weak	strong	[1]saturates at low COT
IR 9.7 (O_3)	Weak	weak	moderate	moderate	weak	moderate	
IR 10.5 (TIR)	Weak	weak	strong	strong	weak	strong	

	Optical thickness COT	Effective radius CRE	Pressure (top) CTP	Fraction CFR	Phase CPHS	Skin T TS	Notes..
IR 12.3 (TIR)	Weak	weak	strong	strong	weak	strong	
IR 13.3 (CO_2)	Weak	weak	strong	strong	weak	strong	

3.2 Assumptions and Limitations

The main assumptions and consequent limitations of the OCA algorithm arise from the simplified cloud model used which in turn is for the most part justified by the limited nature of the observations. Thus the basic OCA model cloud consists of a single layer of zero geometric depth, an optical depth (COT) defined at 0.55 μm and of single phase (ice or water or dust or ash, CPHS). The particle size distribution within the cloud is represented by an effective radius (CRE) and the temperature 'distribution' within the cloud is the ambient temperature at the cloud top pressure (CTP). Finally, the pixel is assumed to be fractionally cloud covered (CFR). A further parameter is the skin temperature (TS) of the underlying surface, not strictly part of the cloud, which is included because of the strong dependence of almost all TIR channels in some cloud conditions.

These assumptions place limitations on the scene types for which cloud parameters might be successfully retrieved. Although of course the idealistic cloud never appears in reality, in practice successful retrievals can be made for a good percentage of real clouds; this can be confirmed with validation exercises (see section 6). Gross deviations from the model are however not suitable for product retrieval.

The most prevalent deviation from the basic single layer model is multi-layer cloud, especially where the layers are widely separated and the lower layer is significantly above the surface. Some 20-40% of cloudy pixels may contain multi-layer cloud. A simple two-layer extension enables the gross effects of many multi-layer systems to be modelled and allows a limited set of lower layer parameters to be retrieved in addition to the upper layer parameters (RD.3). A more thorough treatment of the two-layer system (RD.2) will be implemented in the future and is expected to improved parameter accuracy and availability in these cases.

Cloud with significant geometric structure, especially when combined with high viewing or sun angles, will give rise to large retrieval errors, and, a related problem, shadow effects; neither self-shadowing nor cloud to cloud shadowing is modelled.

A further class of assumptions in the OCA algorithm relate to the non-cloud effects on the radiances. Within OCA only the cloud parameters are retrieved; therefore assumptions are made about atmospheric humidity, temperature, aerosol concentration, ozone concentration, surface emissivity, reflectivity etc. Values for these so called 'model' parameters are derived, for the quickly varying parameters from Numerical Weather Prediction (NWP) sources and

for the more static parameters from available climatologies and datasets. They are therefore of the highest quality and accuracy available in near real time but nevertheless errors remain. Part of the 'optimality' of the OCA scheme comes from appropriate weighting of the measurements in the retrieval. In a system where instrument noise dominates this can be relatively simple since this quantity is well defined and normally scene independent. For cloud retrievals most of the significant 'noise' in the measurements is actually from 'forward modelling errors', i.e. even were one to have the cloud state perfectly defined, there remains errors in the estimation of radiances. These arise from errors in the assumptions made as discussed above and can be both difficult to estimate and state dependent. For example, the error arising from NWP humidity analyses on the water vapour channels may be dependent both on the geographical location and the cloud conditions (above high thick cloud, for example, there is little atmospheric humidity to be in error).

Table 3 lists some of the main limitations to the OCA retrieval at present and indicates possible future enhancements to reduce their effect.

Table 3: Overview of limitations

Limitation	**Effect**	**Future enhancement**
Simple (and IR only) modelling of 2-layer cloud	Poor modelling in TIR and no reflectance channel modelling	Complete fast 2-layer model [RD-2])
Cloud 3D structure	Poor modelling in VIS/NIR	Geometrical correction using high resolution data
Surface emissivity (Land)	Poor modelling in selected TIR (8.7, 3.8, 9.7 μm), thin cloud	Improved dedicated emissivity maps
Surface Reflection (Land)	Poor modelling in VIS for thin-moderate cloud	Improved land albedo maps
Aerosol	Poor modelling in short-wave VIS and high solar / view angles.	Dynamic inclusion of aerosol information and improved radiance modelling
Error characterisation	Less than optimal use of channel information	Continued evaluation and improved modelling of errors.

3.3 Algorithm Basis Overview

This section presents a textual description of the OCA algorithm; details can be found in section 3.5 et. seq.

The OCA algorithm is based on the following components:

- A model of a cloudy atmosphere defined by a set of variable - '**state**' - parameters: **x** = COT, CRE, CTP, CFR, CPHS, TS and a set of fixed - '**model**' - parameters **b** = Atmospheric temperature and gaseous constituents, surface properties etc. Uniquely, the cloud phase, CPHS, is not a continuous variable and takes one of only four values (water, ice, dust or ash).

- A fast radiative transfer model (**RTM**) which, when operated on the state and model parameters, estimates the values of the imager measurements **y**. The operation is denoted by **y**(**x,b**).
- Input **boundary** conditions: a cloud mask (including indication of dust or volcanic ash presence), surface reflectance and emissivities and clear atmosphere radiative properties from a gaseous FASTRTM applied to forecast data.
- Models of **errors** in the measurements and the 'prior to retrieval' values of the state parameters
- A penalty or '**cost**' function, J, which describes the 'distance' (weighted mismatch) between measurements, prior state and the state estimate.
- A technique to minimise the penalty function.

The state and model parameters are described above and in more detail below; it is relevant here only to note again that the algorithm is able to alter the state parameters but the model parameters remain fixed.

The cloud model and the associated RTM are complete and consistent (if also simplistic compared to reality) for single layer cloud treatment. For the representation of multi-layer clouds through a 2 layer system the cloud model *should* be extended (with a COT, CRE, etc for both layers) along with a suitably extended **RTM** (e.g. see RD.2). The current algorithmic implementation however takes a very simplistic albeit effective approach (RD.3). For the lower layer only the temperature of is explicitly modelled by assigning the TS parameter, not to the physical surface temperature, but to an equivalent opaque lower cloud surface. Thus the state parameters of the 2-layer retrieval are the same as the single layer retrieval (the associated prior errors are however different). The single layer RTM still applies in the IR (albeit without correct modelling of the between-layer transmission) but is invalid for the solar channels; these cannot therefore currently be used in the 2-layer retrieval.

The RTM needs to be very fast to achieve real time processing of high resolution imagery and this is achieved with a) the use of lookup tables (LUTs) which store computationally intensive cloud radiative properties, b) pre-calculated atmospheric radiative effects at NWP forecast grid resolution and c) a simple three layer (below cloud, cloud and above cloud) radiative transfer integration.

The cost function in OCA is derived from probability theory, it is technically the negated exponent of the likelihood function. It is a weighted sum of the terms from the mismatch of the measurements from the state calculated values and from the mismatch of the state from the prior assumed values. The weights are derived from the measurement and state prior errors assuming these are normally distributed.

By minimising such a cost function, the optimal balance is found between the information on the state provided by the measurements and that provided by the prior state. For most of the cloud properties in OCA, there is little prior information. The main exceptions are a) TS which originates from NWP data and has low errors and b) CFR which (as discussed above) is assumed to be unity for pixels where cloud has been detected by the CLA algorithm.

The minimisation is aided by starting the iterative procedure as close to the final solution as possible - 'First Guess' state parameters are derived using analogous but highly simplified equations of the RTM.

The minimisation technique used by OCA is a form of the Levenburg-Marquardt iterative algorithm which combines the benefits of 'steepest descent' and Newtonian descent. Steepest descent is, as it suggests, a minimisation method that adjusts the state in the direction that the cost function is most rapidly decreasing. It is robust but can be slow because the step length is not optimised. Newtonian descent on the other hand calculates the exact step length in the case the cost function is already quadratic (that is equivalent to a linear problem in the neighbourhood of the solution); it is however not robust against stepping in false directions when the solution is far from the current state. Iterative descent is halted when the cost function value decreases by less than a preset threshold (or the iteration limit is exceeded). Other such 'convergence' criteria are possible.

Other main features of the algorithm include:

1. Cloud phase can be modified within the descent algorithm. The ice-water absorption differential in the 1.6 μm channel (daytime only, see section 3.1) means that a scene that contains ice cloud but that is being interpreted as water cloud would appear to have very large CRE values. These are identified as being larger than physical limits set on the water CREs and in this case a switch to ice phase is made. The reverse process can occur in the case that ice is assumed and in reality water cloud is present[4]. Note that there are currently no internal switching features to or from dust/ash phases as the absorption characteristics for dust/ash/water, dust/ash/ice are not analogous and appropriate switching mechanisms, if they exist, are not so far identified.
2. The value of the cost function at the end of the iterative process is found to often be a good indicator of the overall quality of the retrieval. This is because the retrieval system is over-constrained in that up to 15 measurements (11 with MSG SEVIRI[5]) are being used to estimate up to 5 state parameters. If the scene does not conform to the cloud-atmosphere model assumed (e.g. there is multi-layer cloud) then it is unlikely that all 15 measurements can be modelled within their expected noise. A retrieval with an unacceptably high cost can be discarded (all products) or potentially rerun (as is currently done in the multi-layer case) with a different underlying cloud model.
3. The OE method naturally provides an estimate of the error in the solution parameters that is a formal combination of assumed measurement and prior state errors, and the

[4] The separation between water and ice in this way appears reasonably successful but there are conditions (notably thin cloud) where such a signal is ambiguous. 'Safe' regimes (ice for CTT < 238 K, water for CTT > 270 K) can be enforced, but the general problem remains. A computationally more expensive but conceptually cleaner and potentially more powerful method, is to perform retrievals for both ice and water and select the result that gives the lowest cost. This approach can theoretically incorporate effects from phase other than the particle size effect which might anyway be of different signs in different channels. A 'try everything' approach (or variants) might also be necessary with the larger channel set compared to SEVIRI (e.g. the 2.2 μm addition) and if more cloud models (e.g. adding a 2-Layer model) were to be considered.

[5] The similar response of some channels means that there are less than 15 (11 for SEVIRI) independent measurements in practice. Similarly, state variables with good prior information mean there are less than 5 independent state variables in practice.

sensitivities of the measurements to the state. The estimate is only valid if the solution cost is acceptably low, i.e. if the cloud model used can be considered valid.

4. Care is taken to handle temperature inversions appropriately. Two main inversion types exist. **Tropopause** inversions ubiquitously present in the NWP temperature profile prevent valid solutions for (albeit rarely occurring) overshooting convective clouds. This is dealt with by presenting the algorithm with a profile with the inversion removed, i.e. temperatures above the tropopause reset to be continually adiabatically cooling. (The original un-modified profile however, *must* be used for the background gaseous IR RTM.) **Boundary layer** BL inversions present a similar problem in that initial CTPs that are *above* the layer mean that solution CTPs *in* the boundary layer cannot be accessed. In addition, NWP model accuracy and model level discretisation means that the inversion tops are not well defined. The solution adopted is to a) detect BL inversions, b) provide profiles modified to give a deeper sharper BL and c) ensure that first guess CTPs lie when appropriate within the BL.

3.4 Algorithm Input

Table 4 summarises the inputs into the OCA process. Main categories are primary data from the sensor, ancillary data from the sensor, data from NWP and derivatives and static datasets. The sections following provide detail.

Type:	Specific:	Notes:
Sensor (dynamic)	FCI channel measurements	In principle all measurements are used, in practice a small number may be effectively excluded because of modelling difficulties
	Geometry	Sun-satellite to determine cloud radiative properties from physical properties
	Geo-location	To determine surface characteristics, interpolate NWP/RTM data
Ancillary dynamic	FCI Cloud Mask	Determines pixels to be processed for cloud products and scene identification with respect to presence of dust or volcanic ash.
NWP dynamic	Profiles, T, Q	Temperature used for cloud IR source function and, with Q, for detecting tropopause and boundary layer inversions
	VIS RTM	2-path transmittances sun-cloud-satellite
	IR RTM	1-path transmittances and layer radiative quantities
Ancillary static	Surface emissivity	Enables calculation of proper IR surface contribution
	Surface reflectance	Enables calculation of proper VIS surface contribution
	Cloud radiative properties	Cloud emissivity (IR), transmissivity and reflectivity as a function of cloud properties and geometry

Table 4 Overview of inputs to OCA

3.4.1 Primary Sensor Data

In principle all FCI imager **channel measurements** are used in the OCA process. Experience with MSG SEVIRI has been that, while some channels are difficult to model and some provide only peripheral information to the cloud state parameters, these difficulties are often eventually surmounted and the robustness of the product enhanced. It is a matter of prudence then that all channels should be made available to the algorithm; channels that are too difficult to model (e.g. currently the 3.9 μm channel on SEVIRI) can be simply down-

weighted in the algorithm to zero by assuming very high noise levels. There is naturally some computational penalty to this, but an advantage is that such channels are 'passively' monitored, i.e. their fit to the retrieved state can be analysed without their having any effect on that state.
Measurements in the range **0.4 - 2.2 μm** are required in reflectance (as a fraction, range 0-1), not normalised by the solar zenith angle:

$\rho_{VIS} = \frac{\pi . L_{VIS}}{F_{sun}}$ where L_{VIS} is the channel radiance and F_{sun} is the TOA solar irradiance integrated over the channel spectral response function (SRF). The reason for not normalising the reflectance is that fixed channel measurement errors then remain valid for all illumination conditions.
Thermal measurements in the range **3.8 - 13.3 μm** are required as equivalent brightness temperatures (BTs).

The three-dimensional **geometry**, satellite zenith angle, solar zenith angle and the satellite-solar relative azimuth is required for each pixel location. For night-time pixels only the satellite zenith angle is used.

Geo-location information is required in order to extract data from the relevant ancillary files. This information is in the form of rectified pixel line-elements coordinates for pixel based ancillary information (e.g. emissivity maps) and latitude / longitude coordinates for NWP based ancillary information.

3.4.2 Ancillary Dynamic Data

Ancillary dynamic data is required from both imagery (pixel based) and NWP based sources.

3.4.2.1 Imagery: Cloud Mask

Current implementations of OCA use the MPEF cloud mask to determine which pixels to process[6] and this is likely to remain the case for the MTG FCI implementation. It is certain at least that cloud type, in the sense of discriminating from meteorological (water/ice) from mineral dust or volcanic ash clouds, will be used to set the cloud type in OCA. Although not yet tested, certain additional features of the scenes analysis (SCE) might be useful to the OCA process, particularly in providing first-guess parameters to improve convergence rates or providing cloud type estimates to determine cloud model choices.

3.4.2.2 NWP: Atmospheric Profiles and RT Quantities

NWP data, currently and for the foreseeable future, from ECMWF, is used to provide the cloud-free atmospheric and (via RTTOV) radiative quantities within which the OCA cloud model is embedded. Because the intrinsic time and space resolution of the NWP data is significantly less than the imagery, the processing of NWP data is made in a separate process prior to OCA (see ATBD L2RTM). Within OCA, NWP atmospheric profiles and RT results are interpolated (linearly) to the time and location of the processing pixel.

[6] Although an OCA-like approach (clear-pixel probabilistic method) could be developed, it is by no means certain to lead to an improved detection accuracy and would require significant amount of development effort.

The principle use of **atmospheric profiles** within OCA (see Table 5) is to supply the pressure dependent temperature used to determine the IR channel cloud source radiance (i.e. the Planck function at cloud temperature). To allow tropopause overshooting, the tropopause level is identified and the temperature profile modified above. Similarly, boundary layer (BL) inversions are identified and adjusted to allow for forecast model accuracy and vertical resolution limitations. These identifications and adjustments are described in Appendix 8. Section 6.4.3 demonstrates the BL issue through A Train validation data. The BL identification will, in the future, make use of the forecast humidity profile in addition to the temperature profile. The profiles are provided on the vertical coordinate system of the RTM model (currently 43 levels of RTTOV). Additionally, various surface parameters from the NWP model are required at the pixel location in OCA.

Table 5: NWP and RT atmospheric quantities required in OCA

NWP	**Dim**	**Description**	**Use**
Temperature	*nlev*	Forecast temperature profile interpolated to pixel	Cloud IR Source function / Subsidence inversion identification
Humidity	*nlev*	Forecast humidity profile interpolated to pixel	Subsidence inversion identification
Skin Temp	-		Surface IR source function
Surface Pressure	-		Cloud physical altitude limit
IR RTM	**Dim**	**Description**	**Use in OCA fast RT model**
$L_{\circ}$	*nirchan*	Clear radiance	cloud-free component
L_{ac}	*nirchan* x *nlev*	Channel upwelling radiances above level	above cloud level[7] upwelling component
L_{bc}	*nirchan* x *nlev*	Channel upwelling radiances below level	below cloud level upwelling component
$L_{ac}^{\downarrow}$	*nirchan* x *nlev*	Channel downwelling radiances above level	above cloud level downwelling component
T_{ac}	*nirchan* x *nlev*	Channel transmittances level to space	for calculating above and below cloud level transmittances
VIS RTM	**Dim**	**Description**	**Use in OCA fast RT model**
T_{2ac}	*nvischan* x *nlev*	2 path transmittances at satellite and solar angles	attenuation of radiance streams

Both IR and VIS **radiative quantities** are derived from the NWP data in a separate processing step prior to OCA processing. The IR requirements are more complex because of the atmospheric emission; in the VIS region only transmittances are required. A further difference is that calculations in the IR are made at the satellite view zenith angle whereas VIS transmittance calculations are made for a combined two-way path, sun-cloud-satellite. The use of these quantities is described in more detail in section 3.5.1; essentially they supply the fixed radiative environment in which the transmitting / absorbing / emitting model OCA cloud is embedded.

[7] The cloud-free RTM that produces these cloud level quantities 'knows nothing' of the cloud properties in the scheme but are pre-calculated at all levels of the RTM model. Interpolation within OCA is used to obtain the quantities for the actual current cloud pressure.

3.4.3 Ancillary Static Data

Two classes of static data apply to the OCA algorithm. The first is pixel based information on surface characteristics necessary as boundary conditions to the OCA fast RT model. The second consists of LUTs to contain the detailed cloud radiative property information.

3.4.3.1 Static Pixel Based Ancillary Data

In the IR channels the surface emitted radiance is defined by the (product of) temperature and the **emissivity**. The temperature is a dynamic variable sourced from the NWP (section 3.4.2.2) and interpolated to the pixel location. The emissivity though is assumed quasi-static and is sourced from pixel based files. Values for all channels are technically required although for very highly absorbing channels (e.g. 6.3 μm) there is practically no surface transmission and the value is irrelevant. Land surface emissivity is currently sourced from a publicly available dataset (CIMSS) and re-projected and spectrally re-sampled for the (in this case MSG SEVIRI) imager. There are plans to derive dedicated emissivity data from the SEVIRI and FCI instruments. Over ocean the emissivity is principally a function of view angle and is currently pre-calculated using the RTTOV model (SIREM) for the appropriate angle. Small wind speed effects are expected and may be modelled in the future.

For the VIS channels the surface source term is determined by the **surface albedo** or reflectance. Currently in OCA this is taken from the operationally produced CRM data which is the period average clear sky reflectance found and is *not* corrected for atmospheric gaseous absorption or aerosol scattering and absorption. The values are used in OCA to determine radiance interactions between cloud and surface and, as most imager absorption and aerosol effects take place in the boundary layer, i.e. between cloud and ground, uncorrected reflectances are probably most appropriate.

3.4.3.2 Cloud Radiative Property LUTs

The CRP LUTs contain reflection, transmission and emission properties of the OCA model clouds which are calculated offline. All the properties are functions of COT and CRE; under current definitions COT ranges from 0.063 to 256 for meteorological cloud types and 0.063 to 8 for dust and ash (preliminary limits to be confirmed), and the CRE range is always type dependent. Most of the properties are also a function of geometry, either a single angle (satellite, ζ_{sat}, or solar zenith, ζ_{sun}) or all three (including the relative azimuth, ψ), see Table 6. The IR and VIS channels share some properties (e.g. diffuse transmission) but some are unique to either (e.g. bi-directional reflectance for VIS; emission for IR). The radiative properties with their physical meaning are:

- **Beam bi-directional reflection** ρ_{BD} is the direct reflection from the cloud layer of the solar beam. It is a function of three-dimensional geometry.
- **Beam transmission**, **direct** T_B is the fraction of the solar beam transmitted unscattered and unabsorbed, through the cloud. Function of just solar angle.
- **Beam transmission, diffuse** T_{FBD} is the fraction of the solar beam transmitted through the cloud having been scattered at least once. This is a three-dimensional

quantity but as OCA assumes a lambertian reflecting underlying surface it is not necessary to retain the directional quality of the radiance and the integrated, or 'flux', version is used (hence the 'F' in the subscript). Similarly, T_{FBD} and T_B are currently used only as a sum in OCA at present.

- **Diffuse transmission** T_D is the transmission of the cloud layer to 'diffuse', i.e. isotropic, radiation. There is a dependency on view angle.
- **Diffuse reflection** ρ_D is the reflection of the cloud layer of isotropic radiation. There is a view angle dependency and this term is used in the IR to reflect downwelling radiation.
- **Diffuse reflection**, **flux** ρ_{FD} is the integrated, flux, version of the diffuse reflection, used in the VIS for cloud - surface reflections.
- **Emissivity** ε_c is the emissivity of the cloud and depends on view angle.

LUTs are available for a variety cloud formulations but OCA currently only uses one LUT based on water cloud properties and one on ice cloud properties.

Implicit to the descriptions of the forward model functionality described is the multi-linear interpolation of the LUTs. If we take for example the equation (6) of section 3.5.2.1.1 (with dependencies made explicit):

$$\rho_{\bullet}^{ic} = \rho_{BD}\left(ic,\tau,\xi_{sun},\xi_{sat},\psi,r_{eff}\right)\mathsf{T}_{2ac}\left(ic,\xi_{sun},\xi_{sat},p_c\right)+\frac{\mathsf{T}_B\left(ic,\tau,\xi_{sun},r_{eff}\right)\mathsf{T}_D\left(ic,\tau,r_{eff}\right)\rho_s\mathsf{T}_{2sfc}\left(ic,\xi_{sun},\xi_{sat}\right)}{\left(1-\rho_s\left(ic\right)\rho_D\left(ic,\tau,r_{eff}\right)\right)}$$

We find LUTs of varying dimensions and dependencies and the following comments should be noted:

- The channel parameter is discrete and no interpolation is implied
- The geometry parameters ξ_{sun},ξ_{sat},ψ are continuous and need interpolation to the pixel values but within a given pixel processing they clearly do not change so that the interpolation parameters (e.g. LUT grid box indices and interpolation factors) can be stored.
- The state parameters τ, r_{eff} are continuous and vary during the pixel minimisation process so that storing e.g. LUT grid box indices will only help if the parameters stay within a single grid box.
- Interpolation factors for the state variables are required for the gradient models.

Table 6: Summary of channel and angle dependencies of LUTs.

Symbol	VIS	IR	ζ_{sat}	ζ_{sun}	ψ
range and resolution[8]:			0–90°, 10°	0–90°, 10°	0–180°, 18°
ρ_{BD}	◆		◆	◆	◆
T_B	◆			◆	
T_{FBD}	◆			◆	
T_D	◆	◆	◆		
ρ_D		◆	◆		
ρ_{FD}	◆				
ε_c		◆	◆		

3.5 Detailed Description

3.5.1 Physical Description

An overview of the physical link between the OCA cloud products and the MTG FCI imager measurements and the method of estimation has been outlined in sections 3.1 and 3.3 respectively. This section expands on these themes, particularly on the OCA fast RTM and the method of cost minimisation. The treatment here is mostly descriptive with some notation introduced to aid familiarity; the mathematical formulation is given in section 3.5.2.

3.5.1.1 The Cloud State Parameters, x

The basic single layer OCA cloud model is shown in Figure 1. The imager pixel is covered with fraction CFR of uniform geometrically thin cloud of optical depth COT, effective radius CRE and is of phase CPHS. It lies at a pressure CTP in the atmosphere. In current practice, as discussed earlier, the value of CFR is constrained to be near unity. These parameters together define the cloud **state x** = [COT,CRE,CTP,CFR,TS[9],CPHS] and are the parameters that are estimated in the algorithm.

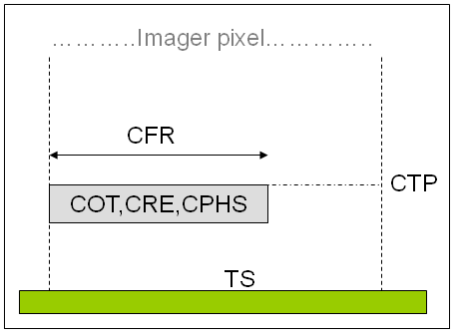

Figure 1: OCA cloud model – single layer

[8] The angular resolution is currently under review and is likely to be increased to adequately capture rainbow and glory scattering features.
[9] TS - skin temperature - is included because of its importance to the IR RT and because the prior information available from NWP over land is often inaccurate

Prior to the retrieval operation we may have some information on the values of the state parameters, known as *a priori*, prior or background information, $\mathbf{x}_a$. The OE methodology allows us to formally include this information by defining a prior cost function (see 3.5.1.6) using $\mathbf{x}_a$ and the covariance of the errors in $\mathbf{x}_a$, $\mathbf{S}_a$. It is the nature of clouds that we actually have little prior knowledge of the state parameters in the observed pixel. Certainly for COT, CRE and CTP there is no information available; $\mathbf{S}_a$ elements for these parameters are therefore set to a high value (e.g. 10^8). For CFR, as discussed earlier, we make the assumption that the cloud detection algorithm has deduced the presence of cloud accurately and further that the cloud cover is complete. $\mathbf{S}_a$ for CFR is therefore set an effective zero value (e.g. 10^{-8}). This is tantamount to removing CFR from the state vector and is a (somewhat false) constraint that will be revisited as the scheme becomes better tuned and / or the extra channels from the FCI provide better constraint on the problem. TS is currently the only variable with genuine prior information available. For ocean pixels a relatively low error of 1.0 K is assumed, for land a higher error, ~5.0 K.

From this one sees that the use of prior information in the standard OCA is currently somewhat limited although experiments using the SEVIRI HRV channel to provide information on CFR is one example of several possibilities available.

As described previously, the same set of state parameters are used to model 2-layer cloud situations (section 3.3). A 2-layer retrieval is made following a single layer retrieval if certain diagnostic criteria are met (see sections 3.5.2.2 and 9.15). In the 2-layer case the cloud model appears as in Figure 2. Note that the fractional cover (implying both layers) is forced to be = 1. The core cloud parameters, COT, CRE and CPHS, apply to the upper layer, and the skin temperature, TS, models the lower layer cloud temperature.

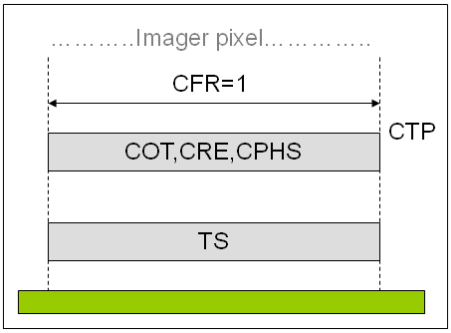

Figure 2 OCA Cloud model – 2-layer

Note that although Figure 2 shows TS as 'elevated' and associated with a cloud layer, as far as the fast RTM (thermal part) is concerned, TS is still the skin temperature. Its ability to act as proxy for the lower cloud temperature arises simply from appropriately set first guess and prior constraint error settings (see sections 3.5.1.7 and 9.17). Note that there is no analogous simplistic treatment for 2-layer reflectance RT, so that all reflectance channels are removed in the 2-layer retrieval (by setting $\mathbf{S}_y$ to 'huge').

3.5.1.2 The Measurements, y

The measurement vector, $\mathbf{y}_m$, constitutes all the single pixel measurements from the sensor; thus 11 for SEVIRI and 15 for MTG FCI. The values are "solar angle uncorrected" reflectance for wavelengths to 3 μm and brightness temperatures thereafter.
The measurements are weighted in the retrieval by their errors, $\mathbf{S}_y$. It is important to note that the definition of error here refers to the ability of the forward model (sections 3.5.1.4 and 3.5.1.5) to reproduce the measurements since this defines how close a fit is expected. Thus the error should in principle include:

- instrument noise
- channel co-registration effects
- effects of deviations from the OCA cloud model
- effects of errors in ancillary model parameters

The **instrument noise** is well characterised but actually the smallest and thus least relevant contribution.

Channel **co-registration** errors arise from channels viewing slightly different ifovs on the earth and therefore potentially different cloud and atmospheric / surface states. The degree of error depends on the homogeneity of the scene and values were estimated in [RD-1] for MSG SEVIRI using the higher resolution ATSR-2 imager for various cloud types. In practice as there is currently no scene type available to OCA a default type = 2 (cumulus) is assumed.
Even were the channels perfectly co-registered, there would remain the inability of the simple **OCA cloud model** to represent the structure of, for example, a cumulus cloud's radiative characters. [RD-1] made an assessment of these effects, again using the dual-view ATSR-2 data. Nadir and 'along-track' (~55^o view angle) measurements were compared and misfits were attributed to non-plane parallel cloud effects. Again, for the current OCA implementation a scene type of cumulus is assumed in setting the so called 'homogeneity' error.

Ancillary **model parameter errors** (section 3.5.1.3) propagate into errors in calculated radiances. The principal parameters here are land surface reflectance for the VIS channels and land surface emissivity and atmosphere temperature / humidity for the IR channels. For the 0.6 μm SEVIRI channel and the shorter wavelength FCI channels, aerosol amounts and types will also be a source of error. These errors are strongly dependent on cloud conditions; the surface reflectance and NWP humidity errors have little effect in deep cloud for example. The effect of surface errors (reflectance, emissivity) can be modelled during the retrieval as the RT for these terms is straightforward. The atmospheric temperature and humidity errors are much harder to model as in principle a complete LW RTM would need to be run. OCA presently includes functionality to include surface reflectance errors in this way. The functionality for emissivity would be equivalently straightforward to add, however, there is no clear way forward for modelling the atmospheric effects at present and these are currently simply ignored.

Correlations between measurement errors, i.e. off-diagonal terms in $\mathbf{S}_y$, are currently neglected. For instrument and probably co-registration noise this is justified, but for the other sources described above correlations are almost certainly non-negligible. Cloud modelling

issues will lead to similar errors amongst the VIS channel group and similar errors in the IR channel group. Correlations from the surface terms would depend on the correlations in the terms errors themselves and these would be hard to estimate. Errors in atmospheric humidity and temperature would reflect in certainly different but correlated errors in the IR channels. It is by no means certain at present how important the specification of correlations is compared to the general level of error (i.e. the diagonals of $\mathbf{S}_y$).

3.5.1.3 The Atmospheric Model Parameters, b

In addition to the cloud **state** parameters, there are the fixed atmospheric parameters necessary to translate the cloud state into imager measurements through the fast RT model. These are traditionally called '**model parameters**' and denoted by the symbol **b**. They include all the ancillary clear sky radiance terms provided by the [AD-3] and the NWP data. Model parameters are not estimated in the algorithm however they are not considered to be error free - in principle the errors in them can be translated into errors in the products. In the current implementation of OCA this is partly achieved.

3.5.1.4 Fast Forward Model: Solar

The 'solar' forward (RT) model in OCA is used to calculate the contribution of the solar beam radiance to the observed channel radiances. Thus it constitutes the entire RT model for channels with wavelengths 0.4 - 2.2 μm, and contributes to the 3.8 μm channel along with the thermal model.
indicates the essential features of the solar fast model for the overcast case.

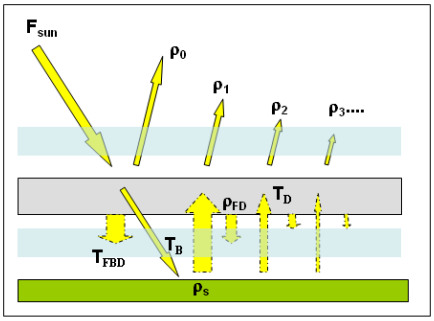

Figure 3: OCA Solar model

Solid delineated arrows at an angle indicate directional radiances and broken vertical arrows denote non-directional irradiances. The solar input, F_{sun}, is part reflected from the cloud (bi-directional reflection, ρ_{BD}) and part transmitted (part as a beam, T_B, and part diffusely, T_{FBD}).
The transmitted radiance is assumed to be isotropically reflected by the surface (ρ_s) and undergoes multiple diminishing reflections (ρ_{FD}) with the overlying cloud layer. At each cloud interaction, some radiance penetrates the cloud in the satellite view direction (T_D). Radiance streams are attenuated by gaseous absorption above and below the cloud; values for which are obtained from the VIS RTM profiles (see section 3.4.2.2) by interpolation to the cloud top pressure.
The calculation for the cloud-free fraction of the pixel is straightforward with only surface reflection and atmospheric attenuation included (not shown).

3.5.1.5 Fast Forward Model: Thermal

The thermal model, Figure 4, is simpler in formulation but includes emission as well as absorption by the atmosphere above and below the cloud. The contributions to the measured radiance are: L_0: the cloud emitted (ε_c) radiance attenuated by the above cloud atmosphere, L_1: the upwelling radiance at cloud base that it transmitted through the cloud (T_D) and attenuated by the atmosphere above the cloud, L_2: radiance reflected from down-welling radiance above the cloud and L_3: radiance emitted by the atmosphere above the cloud. The up- and down-welling radiances are obtained from the IR RT profiles (see section 3.4.2.2) by interpolation to the cloud top pressure. The cloud-free radiance is obtained directly from the IR RT calculation (see Table 5). Radiance terms that include a surface contribution have to be corrected for the pixel resolution surface emissivity (3.4.3.1).

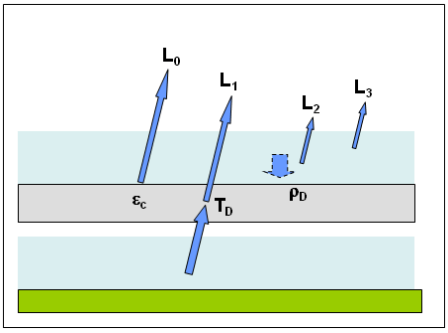

Figure 4: OCA thermal model

In summary for sections 3.5.1.4 and 3.5.1.5: the fast **forward model operates on** the cloud state, **x**, **and** model parameters, **b**, and gives estimates of the imager measurements, **y(x,b)**[10].

3.5.1.6 Cost Function

The 'cost' or 'distance' function, J, which defines the OCA algorithm method is the sum of two parts: the measurement cost (J_m) and the prior cost (J_a)[11].

Given a current estimate of the state **x**, J_m is the weighted squared difference of the observed measurements, $\mathbf{y}_m$, and the values **y**(**x**) (the estimated measurements). The weights are given by the expected errors in the measurements. Formally

$$J_m = (\mathbf{y}_m - \mathbf{y}(\mathbf{x}))^T \mathbf{S}_y^{-1} (\mathbf{y}_m - \mathbf{y}(\mathbf{x})) \quad \textbf{(1)}$$

Similarly, J_a is the weighted squared difference of the prior values of the state, $\mathbf{x}_a$, and **x**; the weights being the expected errors in the prior values.

$$J_a = (\mathbf{x} - \mathbf{x}_a)^T \mathbf{S}_a^{-1} (\mathbf{x} - \mathbf{x}_a)) \quad \textbf{(2)}$$

[10] As **b** is fixed, the forward model often appears as simply **y**(**x**).
[11] The prior is often also referred to as the 'a priori' and 'background'.

A high J therefore indicates that the current state is in 'disagreement' with either the measurements or the prior information or both. At the minimum value of J, the state has been found which gives best agreement with both the prior estimate and the measurements. This is the meaning of the statistical 'optimality' of the OCA method.

If, even at the minimum, the value of J is still high, then something is wrong and, assuming a stable implementation[12], the cause must be that the forward model **y(x)** is unable to represent the measurements, $\mathbf{y_m}$. Since the forward model y is a well behaved function, the corollary is that the state **x** is unable to represent the true state. This is an important characteristic of the OCA algorithm since it enables the detection of many anomalous scenes where the cloud model is not appropriate and retrieved products would therefore potentially be erroneous. Note that there is no *guarantee* that an anomalous scene results in a high J solution, it might be that there is a state that satisfactorily fits the measurements and prior. However the chances that this is so is likely to reduce as the number of (independent) measurements increases over the number of (independent) state parameters; analogously - a straight line can always be made to fit to two points, but not always to three. With OCA therefore we strive to use as many measurements as possible.

3.5.1.7 Minimising the cost function

Minimisation of the cost function involves a 'descent' algorithm which, starting from '**first guess**' estimates of the state parameters, $\mathbf{x_0}$, takes successive steps (or 'iterations'), $\boldsymbol{\delta}\mathbf{x}$, that reduce the cost until either the cost is acceptably small, the cost reduction becomes insignificant, or the iteration limit is exceeded.

The quality of the **first guess** parameter values does not, in general[13], affect the quality of the solution but does usually affect the number of iterations required to find the cost minimum (to 'converge'). OCA therefore takes care to make best possible first estimates of the state parameters before the iterative process begins. These are made in a logical order and a brief summary is given here (for details see 9 APPENDIX: Inversion First Guess procedures):

- **CFR** – Value of 1 taken (see 3.1); better values available in principle from the HRV channel (MSG SEVIRI) or high resolution channels on MTG FCI.
- **CPHS** – when meteorological cloud is indicated by the scenes analysis input it is estimated from the BT difference in the 8.7 and 11 μm channels; otherwise it is set to dust or ash as indicated.
- **COT** – in daytime conditions estimated from a CFR corrected 0.8 μm channel making allowance for the estimated CPHS. The 0.8 μm channel is only slightly influenced by the, so far, undefined CRE and CTP. In night time conditions a regression on IR channels is used.

[12] i.e. no gross errors in the measurements or the prior state or their error characterisation and a robust minimisation scheme.

[13] One significant example, however, where the first guess is very important is the case of stratiform cloud under subsidence inversions where cost function minima can exist for solutions below the inversion and above. Although only one is the true minimum, a simple descent algorithm is unable to 'jump' over the high cost region of the inversion from one to the other. Ensuring the first guess is in the correct region solves the problem.

- **CRE** – in daytime conditions estimated from a CFR corrected NIR channel (1.6 μm with MSG SEVIRI) making allowance for the value of the first guess COT. In night time conditions a static value dependent on CPHS is used.
- **CTP** – estimated from the COT and CRE corrected 11 μm channel.
- **TS** – taken from the NWP data.

Although it is not proven, experience suggests that the cost functions found with MSG SEVIRI measurements and the OCA cloud model state definition are relatively 'well behaved'. This means that there are generally few instances of multiple minima or other complex features that would require the use of sophisticated search algorithms to find the true minimum (see note[13]). OCA therefore operates a straightforward Levenberg-Marquardt descent algorithm (see section 3.3) which combines steepest descent and Newtonian methods.

Steepest descent (SD) involves stepping in the direction in *x*-space that is in the steepest 'downhill' direction, $-\mathbf{J}' = -\frac{\partial \mathrm{J}}{\partial \mathbf{x}}$. Such steps will always be in the correct direction although as the length of the step is not determined and may be too far (stepping past the minimum) or too short (needing many iterations). **Newtonian descent** (ND) on the other hand uses a step that is Newton's root finding method for the equation $\mathbf{J}' = \mathbf{0}$ which is the condition expected at any minimum. The step is thus $\frac{-\mathbf{J}'}{\mathbf{J}''}$ and, if J is a quadratic function of **x**, as it would be if all errors are purely Gaussian and the RT is linear in **x**, then one step finds exactly the minimum. It is because the RT is not in practice completely linear that these two descent methods are combined with a mechanism to alter the balance between them. Thus the Levenberg-Marquardt step is given by

$$\boldsymbol{\delta x} = -\left(\mathbf{J}'' + \alpha \mathbf{I}\right)^{-1} \mathbf{J}' \qquad \textbf{(3)}$$

where the control variable α is varied to shift between SD and ND; α very small is equivalent to ND. Adjustment of α is made according to the success of the last step made: if the step is successful (i.e. lowers the value of J) then α is reduced (by e.g. a factor of 10) because it is assumed the minimum is nearer and the problem more linear. If the step is unsuccessful in that the value of J would increase, the step is not made and α is increased.

The initial value for α is set as a scaled value of the 'average' size of $\mathbf{J}''$ at the first guess state (given by the sum of its diagonals; the trace of $\mathbf{J}''(\mathbf{x_0})$) which indicates the curvature of the cost function. A factor, MQ_{start}, relates the initial value of α to this size; a value of MQ_{start} = 0.01 is currently used, thus: $\alpha_{start} = MQ_{start} \times TRACE(\mathbf{J}''(\mathbf{x_0}))$.

The **state** variables are all **bounded** in the values they can take, either by hard limits (CFR, CTP) or softer limits defined by LUT ranges (COT, CRE). The question arises as to an appropriate strategy in the event that a step would take a parameter(s) over boundary limits. Two possibilities exist: the step is not taken and a shift towards a safer SD made or the step is taken but the relevant parameters take on the boundary values. OCA adopts the second strategy with the reasoning that some boundary values are not unlikely (e.g. CFR=1 (or 0); CTP=$P_{tropopause}$ or $P_{surface}$ etc.). For COT, the boundary values determined by the LUTs (plus

some extrapolation) are not strictly physical limits[14], but they are effectively limits of sensitivity of the measurements so the implied restriction is not significant. Boundary limits in **CRE** are a little different in that in the current OCA certain boundary crossings are taken to be indicative of an incorrectly assumed **cloud phase**. Crossing the lower CRE boundary of the ice phase LUT is taken to mean the cloud is actually water phase and crossing the upper boundary of the water phase LUT that the cloud is actually ice. This is to a degree successful because the main driver of phase identification within the MSG SEVIRI measurements is the absorption properties at 1.6 μm and the 'measurement space' occupied by, for example, the 0.8, 1.6 μm reflectances (c.f. Nakajima and King diagram), lie mostly separated for the two phases. It is also a computationally efficient method especially if a reasonably accurate first guess value is achieved, limiting the number of pixels where a crossing is necessary. A theoretically cleaner method is to run the minimisation twice and take the lowest cost to indicate phase. It would have at least two advantages:

- No dependency on somewhat artificially imposed LUT boundaries in CRE (currently 23 μm for water (upper) and 10 μm (lower) for ice (depending on ice model used)). Evidence already exists that large water phase CREs in developed maritime stratocumulus are being incorrectly assigned ice phase despite high cloud temperatures.
- More robust to conflicting signals. The 8.7 μm channel response to incorrect phase assumption is in the reverse direction to the 1.6 μm channel in that ice should 'look like' *small* water CRE, not large. The strength of the signal in 1.6 μm compared to 8.7 μm seems to largely override this potential problem in the current OCA method. With the greater numbers of CRE sensitive channels with the MTG FCI, there may be a stronger imperative to implement the more general method.

Clearly there is a computational cost to pay for the proposed method[15], but this might be minimised by eliminating the second run for 'safe' cases (e.g. ice determined by 11 μm BT < 230K) and starting the second phase minimisation at first guess values of COT[16] , CTP, CFR and TS taken from the first result.

The mathematical operations, particularly the matrix inverses, involved in the calculation of $\mathbf{J}'$ and $\mathbf{J}''$ are subject to rounding errors. Because of the very different state parameters and sensitivities of the measurements, the minimisation can be affected and OCA attempts to rectify this by **scaling the parameters**. For example, the entire range of CFR is 1.0 and a unit change in CFR leads to very high changes in measurement values. For CTP, on the other hand, a unit change (1 hPa) has a very small effect on the measurements. OCA therefore scales CFR by x100 so that unit change, in the mathematical code, has a correspondingly smaller effect. Because the channel sensitivities vary widely depending on cloud and surface conditions it is not possible with constant scaling factors to keep the entire problem well scaled, but the issue is not a critical one and the adopted scaling appears to be adequate.

[14] Meteorological clouds with COT less than 0.1 or greater than 256 are technically feasible; the LUT ranges for dust and ash will be eventually determined so that real values are unlikely to exceed them.
[15] And because of this it the strategy would have to be modified for volcanic ash and dust because of their comparatively rare occurrence rates.
[16] COT would have to be adjusted to reflect the often very different channel responses to ice and water COTS; highly forward scattering ice particles (e.g. plates), for example have high optical depth for the same reflectivity as aggregate ice particles.

A related issue is the representation of **optical depth** in **logarithmic** space. This retains sensitivity to the COT parameter for low COT and keeps the sensitivity of measurements to COT linear over a larger range. The corresponding gradients of RT parameters (see sections 3.5.2.1.2 and 3.5.2.1.4) calculated from the discrete LUT table positions are therefore more accurate.

The iterative minimisation must be stopped at some point and this is determined by the **convergence criteria**. OCA uses a simple criteria that gives a threshold on the absolute change in cost: if, for an iteration, the calculated change in cost is below this value, the minimisation is said to have converged. The threshold is currently set to 1.0 and this is applied to the total cost $J = J_m + J_a$; the threshold per *degree of freedom* in the system is therefore of order 1/(11+5). Increasing the number of channels from the MSG SEVIRI implementation for MTG FCI should imply a somewhat higher threshold under this definition.

3.5.2 Mathematical Description

3.5.2.1 Radiative Transfer

3.5.2.1.1 Solar Forward Model

Section 3.5.1.4 and Figure 3 describes the solar fast radiative transfer scheme. The derivation here is made directly in un-normalised reflectance rather than radiance. The direct solar reflection and reflectance from subsequent cloud-surface interactions from overcast conditions for channel *i* can be written as (neglecting atmospheric attenuation for the moment)

$$\rho_{\bullet}^{i} = \rho_{BD}^{i}(\mathbf{x},\xi_{sun},\xi_{sat},\psi) + \mathsf{T}_{B}^{i}(\mathbf{x},\xi_{sun})\rho_{s}^{i}\mathsf{T}_{D}^{i}(\mathbf{x},\xi_{sat}) + \mathsf{T}_{B}^{i}(\mathbf{x},\xi_{sun})\rho_{s}^{i2}\mathsf{T}_{D}^{i}(\mathbf{x},\xi_{sat})\rho_{D}^{i}(\mathbf{x},\xi_{sat}) + \mathsf{T}_{B}^{i}(\mathbf{x},\xi_{sat})\rho_{s}^{i3}\mathsf{T}_{D}^{i}(\mathbf{x},\xi_{sat})\rho_{D}^{i2}(\mathbf{x},\xi_{sat}) + \ldots \quad \textbf{(4)}$$

The direct term is attenuated by the two-path absorption above the cloud layer, T_{2ac}^{i}, and the first transmitted-surface reflected term by two-path absorption of the whole atmosphere, T_{2sfc}^{i}. Subsequent multiple reflections cloud-surface are attenuated only by the path from cloud to ground plus the ground to space but for practical reasons the whole atmosphere transmission is used[17].

Thus equation 4 becomes (dropping channel superscript and state, angle dependencies for clarity):

$$\rho_{\bullet} = \rho_{BD}\mathsf{T}_{2ac} + \mathsf{T}_{B}\rho_{s}\mathsf{T}_{D}\mathsf{T}_{2sfc} + \mathsf{T}_{B}\rho_{s}^{2}\mathsf{T}_{D}\rho_{D}\mathsf{T}_{2sfc} + \mathsf{T}_{B}\rho_{s}^{3}\mathsf{T}_{D}\rho_{D}^{2}\mathsf{T}_{2sfc} + \ldots \quad \textbf{(5)}$$

This simplifies via the geometric series to

[17] For most solar channels the majority of the attenuation will be anyway below cloud layer. Further, the higher order multiple reflections very quickly become insignificant.

$$\rho_{\bullet} = \rho_{BD}\mathsf{T}_{2ac} + \frac{\mathsf{T}_B\mathsf{T}_D\rho_s\mathsf{T}_{2sfc}}{(1-\rho_s\rho_D)} \quad \textbf{(6)}$$

From the cloud-free part of the pixel the reflectance is

$$\rho_{\circ} = \rho_s\mathsf{T}_{2sfc} \quad \textbf{(7)}$$

and the pixel reflectance is

$$\rho = \mathrm{f}\rho_{\bullet} + (1-\mathrm{f})\rho_{\circ} \quad \textbf{(8)}$$

3.5.2.1.2 Solar Jacobian Model

The jacobian of the RT solar model is the partial derivative of the reflectances with respect to state and model parameters. The jacobian w.r.t. state parameters[18] is required in the descent algorithm (section 3.5.1.7) and the jacobian w.r.t model parameters is needed to either establish product errors arising from model parameter error or to add equivalent noise to the measurements to reflect this uncertainty.
The jacobian *w.r.t.* CFR is, from 8,

$$\mathbf{K}_{\mathrm{f}} = \frac{\partial\boldsymbol{\rho}}{\partial\mathrm{f}} = \boldsymbol{\rho}_{\bullet} - \boldsymbol{\rho}_{\circ} \quad \textbf{(9)}$$

Jacobians *w.r.t.* other parameters are generally

$$\mathbf{K}_{\mathrm{x}} = \frac{\partial\boldsymbol{\rho}}{\partial\mathbf{x}} = \mathrm{f}\frac{\partial\boldsymbol{\rho}_{\bullet}}{\partial\mathbf{x}} + (1-\mathrm{f})\frac{\partial\boldsymbol{\rho}_{\circ}}{\partial\mathbf{x}}$$

but, as cloud free reflectances have no dependency on cloud parameters

$$\mathbf{K}_{\mathrm{x}} = \frac{\partial\boldsymbol{\rho}}{\partial\mathbf{x}} = \mathrm{f}\frac{\partial\boldsymbol{\rho}_{\bullet}}{\partial\mathbf{x}} \quad \textbf{(10)}$$

Clear reflectances may have dependency on the model parameters so that, for the surface reflectance for example,

$$\mathbf{K}_{\boldsymbol{\rho}\mathrm{s}} = \frac{\partial\boldsymbol{\rho}}{\partial\boldsymbol{\rho}_{\mathrm{s}}} = \mathrm{f}\frac{\partial\boldsymbol{\rho}_{\bullet}}{\partial\boldsymbol{\rho}_{\mathrm{s}}} + (1-\mathrm{f})\frac{\partial\boldsymbol{\rho}_{\circ}}{\partial\boldsymbol{\rho}_{\mathrm{s}}} \quad \textbf{(11)}$$

The following presents the expressions for the gradient terms without the tedious workings. These are deferred to the APPENDIX: Gradient model workings, which serves as a reference. Note that gradients (*w.r.t.* COT and CRE) of the cloud radiative properties such as T_D etc are obtained from the LUTs for these variables as part of the LUT interpolation.

[18] Note that there is no jacobian w.r.t. the discrete variable cloud phase, CPHS.

Equation 6 for the overcast reflectance we write in shorthand:

$$\boldsymbol{\rho_{\bullet} = \rho_{BD} T_{ac} + S} \tag{12}$$

to facilitate the jacobian calculations.

The jacobians *w.r.t.* **CRE** (a prime here indicates a derivative *w.r.t.* CRE):

$$\mathbf{K_{re}} = \mathrm{f}\frac{\partial \boldsymbol{\rho_{\bullet}}}{\partial \mathbf{r_e}} = \mathrm{f}\left\{\boldsymbol{\rho'_{BD} T_{2ac}} + \mathbf{S}\frac{(\mathbf{T_D T'_B + T'_D T_B})}{\mathbf{T_B T_D}} + \mathbf{S}\frac{\boldsymbol{\rho_s \rho'_D}}{(\mathbf{1-\rho_s \rho_D})}\right\} \tag{13}$$

It is numerically safer (in the case of zero transmission cloud) to rewrite (and code) 13 in the form

$$\mathbf{K_{re}} = \mathrm{f}\frac{\partial \boldsymbol{\rho_{\bullet}}}{\partial \mathbf{r_e}} = \mathrm{f}\left\{\boldsymbol{\rho'_{BD} T_{2ac}} + \vec{\mathbf{S}}(\mathbf{T_D T'_B + T'_D T_B}) + \mathbf{S}\frac{\boldsymbol{\rho_s \rho'_D}}{(\mathbf{1-\rho_s \rho_D})}\right\} \;\; ; \;\; \text{where } \vec{\mathbf{S}} = \frac{\mathbf{S}}{\mathbf{T_B T_D \rho_s}} \tag{14}$$

The jacobian *w.r.t.* **COT** is given by equation 15 with the primed variables instead indicating a derivative *w.r.t.* COT:

$$\mathbf{K}_{\tau} = \mathrm{f}\frac{\partial \boldsymbol{\rho_{\bullet}}}{\partial \boldsymbol{\tau}} = \mathrm{f}\left\{\boldsymbol{\rho'_{BD} T_{2ac}} + \vec{\mathbf{S}}(\mathbf{T_D T'_B + T'_D T_B}) + \mathbf{S}\frac{\boldsymbol{\rho_s \rho'_D}}{(\mathbf{1-\rho_s \rho_D})}\right\} \tag{15}$$

The jacobian of the reflectance *w.r.t.* **CTP** follows from the dependency of the two path transmission,

$$\mathbf{K_{pc}} = \mathrm{f}\frac{\partial \boldsymbol{\rho_{\bullet}}}{\partial \mathbf{p_c}} = \mathrm{f}\frac{\partial \boldsymbol{\rho_{\bullet}}}{\partial \mathbf{T_{2ac}}}\frac{\partial \mathbf{T_{2ac}}}{\partial \mathbf{p_c}} = \mathrm{f}\boldsymbol{\rho_{BD}}\frac{\partial \mathbf{T_{2ac}}}{\partial \mathbf{p_c}} \tag{16}$$

where $\frac{\partial T_{2ac}}{\partial p_c}$ is available from the forward model interpolation procedure.

Finally the jacobian *w.r.t.* the surface reflectance model parameter ρ_s :

$$\mathbf{K_{rs}} = \mathrm{f}\frac{\partial \boldsymbol{\rho_{\bullet}}}{\partial \boldsymbol{\rho_s}} + (1-\mathrm{f})\frac{\partial \boldsymbol{\rho_{\circ}}}{\partial \boldsymbol{\rho_s}} = \mathrm{f}\mathbf{S}\left[\frac{1}{\boldsymbol{\rho_s}} + \frac{\boldsymbol{\rho_D}}{(\mathbf{1-\rho_s \rho_D})}\right] + (1-\mathrm{f})\mathbf{T_{2sfc}} \tag{17}$$

3.5.2.1.3 Thermal Forward Model

Section 3.5.1.5 and Figure 4 describes the thermal fast radiative transfer scheme. The model is of course entirely consistent with the solar model but takes a rather different form because of the lack of a beam source and the presence of significant atmospheric emission.

The overcast radiance is given by

$$L_{\bullet}^{i} = L_{bc}^{i}(p_c, \xi_{sat})\mathsf{T}_D^{i}(\mathbf{x}, \xi_{sat})\mathsf{T}_{ac}^{i}(\xi_{sat}) + B^{i}(T(p_c))\varepsilon_c^{i}(\mathbf{x}, \xi_{sat})\mathsf{T}_{ac}^{i}(\xi_{sat}) + \\ + L_{ac}^{\downarrow i}(p_c, \xi_{sat})\rho_D^{i}(\mathbf{x}, \xi_{sat})\mathsf{T}_{ac}^{i}(\xi_{sat}) + L_{ac}^{i} \quad \textbf{(18)}$$

The four contributing terms are respectively: transmission of the radiance upwelling at cloud level ("L_0" in Figure 4), emission from the cloud (L_1), reflection of the radiance downwelling at the cloud level (L_2) and emission from the atmosphere above the cloud (L_3).

In the simplified notation omitting channel index and state and angle dependencies,

$$L_{\bullet} = L_{bc}\mathsf{T}_D\mathsf{T}_{ac} + B(T(p_c))\varepsilon_c\,\mathsf{T}_{ac} + L_{ac}^{\downarrow}\rho_D\mathsf{T}_{ac} + L_{ac} \quad \textbf{(18a)}$$

The cloud-free radiance, $L_{\circ}$, is a function of the state parameter TS and its initial value is given directly by the ancillary LWRTM data based on the NWP fields and on the NWP TS^0 in particular. Its value during the iterative minimisation, where TS can vary, is made noting that TS only affects the surface emitted term and assuming linearity of the Planck function for the expected range of temperature deviations from the NWP value,

$$L_{\circ}(T_s) = L_{\circ}(T_s^0) + (T_s - T_s^0)\left.\frac{\partial B(T_s)}{\partial T_s}\right|_{T_s^0}\varepsilon_s\mathsf{T}_{sfc} \quad \textbf{(19)}$$

The radiances upwelling at cloud base are similarly affected by a change in TS:

$$L_{bc}(T_s) = L_{bc}(T_s^0) + (T_s - T_s^0)\left.\frac{\partial B(T_s)}{\partial T_s}\right|_{T_s^0}\varepsilon_s\mathsf{T}_{ps\to pc} \quad \textbf{(20)}$$

As with the solar model, the pixel radiance is given by

$$L = \mathrm{f}L_{\bullet} + (1-\mathrm{f})L_{\circ} \quad \textbf{(21)}$$

3.5.2.1.4 Thermal Jacobian Model

The jacobian of the RT thermal model is the partial derivative of the radiances with respect to state and model parameters.

The jacobian *w.r.t.* CFR is, from 21,

$$\mathbf{K_f} = \frac{\partial \mathbf{L}}{\partial \mathrm{f}} = \mathbf{L_\bullet} - \mathbf{L_\circ} \tag{22}$$

Jacobians *w.r.t.* other parameters are generally

$$\mathbf{K_x} = \frac{\partial \mathbf{L}}{\partial \mathbf{x}} = \mathrm{f}\frac{\partial \mathbf{L_\bullet}}{\partial \mathbf{x}} + (1-\mathrm{f})\frac{\partial \mathbf{L_\circ}}{\partial \mathbf{x}} \quad .$$

and as COT, CRE and CTP do not affect the clear radiance, jacobians *w.r.t.* these parameters are as follows:

$$\mathbf{K_\tau} = \mathrm{f}\frac{\partial \mathbf{L_\bullet}}{\partial \tau} = \mathrm{f}\mathsf{T}_{\mathbf{ac}}\left[\mathbf{L_{bc}}\mathbf{T_D'} + \mathbf{B}(\mathrm{T}(\mathrm{p_c}))\right]\boldsymbol{\varepsilon}_\mathbf{c}' + \mathbf{L}_{\mathbf{ac}}^{\downarrow}\boldsymbol{\rho}_\mathbf{D}' \tag{23}$$

$$\mathbf{K_{re}} = \mathrm{f}\frac{\partial \mathbf{L_\bullet}}{\partial r_e} = \mathrm{f}\mathsf{T}_{ac}\left[\mathbf{L_{bc}}\mathbf{T_D'} + \mathbf{B}(T(p_c))\right]\boldsymbol{\varepsilon}_\mathbf{c}' + \mathbf{L}_{\mathbf{ac}}^{\downarrow}\boldsymbol{\rho}_\mathbf{D}' \tag{24}$$

$$\mathbf{K_{pc}} = \mathrm{f}\frac{\partial \mathbf{L_\bullet}}{\partial p_c} = \mathrm{f}\left\{\frac{\partial \mathbf{L_{ac}}}{\partial p_c} + \frac{\partial \mathsf{T}_{ac}}{\partial p_c}\left[\mathbf{L_{bc}}\mathbf{T_D} + \mathbf{B}(T(p_c))\boldsymbol{\varepsilon}_\mathbf{c} + \mathbf{L}_{\mathbf{ac}}^{\downarrow}\boldsymbol{\rho}_\mathbf{D}\right]\right\} + \quad .$$

$$\mathrm{f}\mathsf{T}_{ac}\left[\frac{\partial \mathbf{L_{bc}}}{\partial p_c}\mathbf{T_D} + \frac{\partial \mathbf{B}(T(p_c))}{\partial p_c}\boldsymbol{\varepsilon}_\mathbf{c} + \frac{\partial \mathbf{L}_{\mathbf{ac}}^{\downarrow}}{\partial p_c}\boldsymbol{\rho}_\mathbf{D}\right] \tag{25}$$

TS affects overcast and clear radiances and so the jacobian becomes

$$\frac{\partial \mathbf{L}}{\partial T_s} = \mathrm{f}\frac{\partial \mathbf{L_\bullet}}{\partial T_s} + (1-\mathrm{f})\frac{\partial \mathbf{L_\circ}}{\partial T_s} = \mathrm{f}\mathsf{T}_{ac}\frac{\partial \mathbf{L_{bc}}}{\partial T_s}\mathsf{T}_D + (1-\mathrm{f})\frac{\partial \mathbf{L_\circ}}{\partial T_s} \tag{26}$$

and as for equations 18 and 19 we obtain

$$\frac{\partial \mathbf{L_\circ}}{\partial T_s} = \left.\frac{\partial \mathbf{B}(T_s)}{\partial T_s}\right|_{T_s^0}\boldsymbol{\varepsilon}_\mathbf{s}\mathsf{T}_{sfc} \quad \text{and} \quad \frac{\partial \mathbf{L_{bc}}}{\partial T_s} = \left.\frac{\partial \mathbf{B}(T_s)}{\partial T_s}\right|_{T_s^0}\boldsymbol{\varepsilon}_\mathbf{s}\mathsf{T}_{sfc\to pc} \tag{27}$$

3.5.2.2 Cost Function and Minimisation

The working definition of OCA is that the probability that the cloud state takes a value x conditional on the given measurements, y_m, prior information x_b and model parameters, b, is[19]

$$P(\mathbf{x}) \propto \exp\left[-(\mathbf{y}(\mathbf{x})-\mathbf{y_m})^{\mathrm{T}}\mathbf{S_y^{-1}}(\mathbf{y}(\mathbf{x})-\mathbf{y_m})\right]\times\exp\left[-(\mathbf{x}-\mathbf{x_b})^{\mathrm{T}}\mathbf{S_x^{-1}}(\mathbf{x}-\mathbf{x_b})\right]\times$$
$$\times\exp\left[-(\mathbf{b_t}-\mathbf{b})^{\mathrm{T}}\mathbf{S_b^{-1}}(\mathbf{b_t}-\mathbf{b})\right] \tag{28}$$

[19] The assumptions being normally distributed errors with no correlations between errors in prior, measurements and model parameters

Instead of maximising the probability, it is cheaper and equivalent to minimise the negative sum of the exponents, that is J:

$$\mathrm{J}(\mathbf{x}) = (\mathbf{y}(\mathbf{x}) - \mathbf{y}_\mathbf{m})\mathbf{S}_\mathbf{y}^{-1}(\mathbf{y}(\mathbf{x}) - \mathbf{y}_\mathbf{m}) + (\mathbf{x} - \mathbf{x}_\mathbf{b})^\mathrm{T}\mathbf{S}_\mathbf{x}^{-1}(\mathbf{x} - \mathbf{x}_\mathbf{b}) \quad \textbf{(29)}$$

The model parameter (3rd) term has been omitted in equation 29 as it is independent of **x**; it adds a constant value to J and is not relevant to the minimisation process (but is to quality threshold decisions based on J).

As discussed in section 3.5.1.7, the Levenburg-Marquardt descent algorithm is used to find the minimum value and it required first and second derivatives of J *w.r.t.* **x**.

$$\mathbf{J}' = \frac{\partial \mathrm{J}}{\partial \mathbf{x}} = \mathbf{K}_\mathbf{x}^\mathrm{T}\mathbf{S}_\mathbf{y}^{-1}(\mathbf{y}(\mathbf{x}) - \mathbf{y}_\mathbf{m}) + \mathbf{S}_\mathbf{x}^{-1}(\mathbf{x} - \mathbf{x}_\mathbf{b}) \quad \textbf{(30)}$$

and

$$\mathbf{J}'' = \frac{\partial^2 \mathrm{J}}{\partial \mathbf{x}^2} = \mathbf{K}_\mathbf{x}^\mathrm{T}\mathbf{S}_\mathbf{y}^{-1}\mathbf{K}_\mathbf{x} + \mathbf{S}_\mathbf{x}^{-1} \quad \textbf{(31)}$$

where, in equation 31, $\mathbf{K}_\mathbf{x}'$ is approximated as zero (i.e. the RT model is linear in **x**). As the use of J'' is in the Newtonian regime of the descent which assumes linearity, this is not really a limitation.

Figure 5 schematically represents the implementation of the Marquardt descent algorithm in OCA. Background yellow boxes show the larger structure of the scheme; the iterative loop, the phase change and 2-layer functions and the steepest descent - Newton adjustment mechanism. Red boxes show decisions (yes/no) and blue boxes show the application of the preceding equations ('Calc') or simpler variable assignments ('Set'). Note that the blue boxes often contain equivalent operations; modular implementation is here possible. The green box highlights the point at which the state vector is actually incremented according to the calculated step and confirmation that the solution cost will reduce.

The scheme exits when a) too many phase changes have occurred (rarely happens), b) the iteration count goes above the set limit or c) successful convergence is achieved.

For clarity and brevity here, the mathematical description of the actions in the boxes of Figure 5 are detailed in Appendix 0.

3.5.2.3 Output parameters

At the end of the minimisation process there is some post processing that is demanded because of the 2-layer cloud retrieval possibility. If the single layer run was successful (solution cost below threshold), then the output stages are straightforward: output products are directly the state parameter values at the solution and the error analysis for the products is the classical OE (see section 3.5.2.4). The additional ash and dust mass loadings, if output explicitly, must be calculated according to the microphysical model used (in LUT generation)

but will be a simple function of COT and CRE (c.f. water paths as 5/9 COT.CRE for meteorological clouds.
If however, the 2-layer model retrieval was run in response to the diagnostics of the single layer result, then some further interpretation of the result is required to obtain 2-layer products and associated errors. In brief this includes:

- Select the best model: 2-layer result or single; based on weighted solution costs
- If 2-layer:
    - Extract the lower layer COT. This is achieved by subtracting the retrieved COT (by definition the upper layer value) from the single layer result[20]
    - Correct the TS (lower layer cloud proxy temperature) using the lower layer COT. This converts TS from representing the temperature of an opaque lower cloud layer to that of a non-opaque, i.e. transmitting cloud.
    - Convert the corrected TS to lower cloud CTP. This is by reference to the forecast temperature profile and includes allowance for any boundary layer inversions present.
    - Convert the expected error in TS into expected error in lower layer CTP via the temperature / height lapse rate
    - The lower layer COT error is currently awaiting definition.

Details of these procedures are given in Appendix 10.

3.5.2.4 Error Analysis

[RD-1] gives a detailed analysis of the error characteristics of the retrieved products broken down into the contributions from measurement error, $\mathbf{S_M}$, 'null space' error, $\mathbf{S_N}$, and model parameter error, $\mathbf{S_B}$. Null space error originates from the fundamental limitations of the observations, for example COT can never be determined absolutely accurately as the measurements are not able to disentangle unambiguously the effects of other parameters (both state and model). This would be the case even with error-free measurements; with errors on the measurements an additional error on the products is introduced. These terms together combine, $\mathbf{S_T} = \mathbf{S_M} + \mathbf{S_N}$, to give the standard OE error equation[21],

$$\mathbf{S_T} = (\mathbf{S_x^{-1}} + \mathbf{K_x^T S_y^{-1} K_x})^{-1} \quad \textbf{(32)}$$

where $\mathbf{K_x}$ is evaluated at the solution. Note from equation 31 that therefore

$$\mathbf{S_T} = \mathbf{J''^{-1}} \quad \textbf{(33)}$$

Although the off-diagonal elements of $\mathbf{S_{\hat{x}}}$ contain interesting information on the correlations between parameter errors, it is normal to quote only the square-root of the diagonal element *i* as the standard deviation error in parameter *i*.

[20] The single layer result is of course obtained under the false assumption that there is only one layer of one phase, but despite this implicit error, the method is useful.
[21] SB is not included in the standard OE error equation and must be calculated separately.

When the effect of a model parameter error is well defined then its contribution to the retrieval error, $\mathbf{S_B}$, is similarly available. Given the retrieved parameters sensitivity to the measurements of $\mathbf{D_y} = \frac{\partial \hat{\mathbf{x}}}{\partial \mathbf{y}}$, the measurements sensitivity to model parameters, $\mathbf{x_b}$, of $\mathbf{K_b} = \frac{\partial \mathbf{y}}{\partial \mathbf{x_b}}$ and the error covariance of the model parameters, $\mathbf{S_b}$, then the retrieved parameter error covariance resulting from uncertain model parameters is

$$\mathbf{S_B} = \left(\mathbf{D_y K_b}\right)\mathbf{S_b}\left(\mathbf{D_y K_b}\right)^{\mathrm{T}} \tag{34}$$

As

$$\mathbf{D_y} = (\mathbf{S_x} + \mathbf{K S_y^{-1} K^T})^{-1}\mathbf{K S_y^{-1}} = \mathbf{S_T K S_y^{-1}} \tag{35}$$

We have

$$\mathbf{S_B} = \left(\mathbf{S_T K_b S_y^{-1} K_b}\right)\mathbf{S_b}\left(\mathbf{S_T K_b S_y^{-1} K_b}\right)^{\mathrm{T}} \tag{36}$$

Equation 36 can be applied straightforwardly for the surface reflectance model parameter, r_s, where the sensitivity of the measurements $\mathbf{K_{rs}}$ ($=\mathbf{K_b}$ in 36) is formally available (section 3.5.2.1.2). The error covariance of the surface reflectances $\mathbf{S_{rs}}$ ($=\mathbf{S_b}$ in 36), may not be well known though.

An alternative to calculating the error induced by errors in model parameters is to calculate the 'equivalent model parameter noise' (**EQMPN**) on the measurements and include this in the measurement error during the retrieval.

The EQMPN component is

$$\mathbf{S_{yb}} = \mathbf{K_b S_b K_b^T} \tag{37}$$

and since $\mathbf{K_b}$ generally depends on the cloud state this is added to the static measurement error components during the iterative process,

$$\mathbf{S_y} = \mathbf{S_{y0}} + \mathbf{S_{yb}} \tag{38}$$

This method has the potential advantage that the minimisation process then does not attempt to over-fit measurements. It should be noted that *both* equations 36 and 38 should not be applied for the same model parameter.

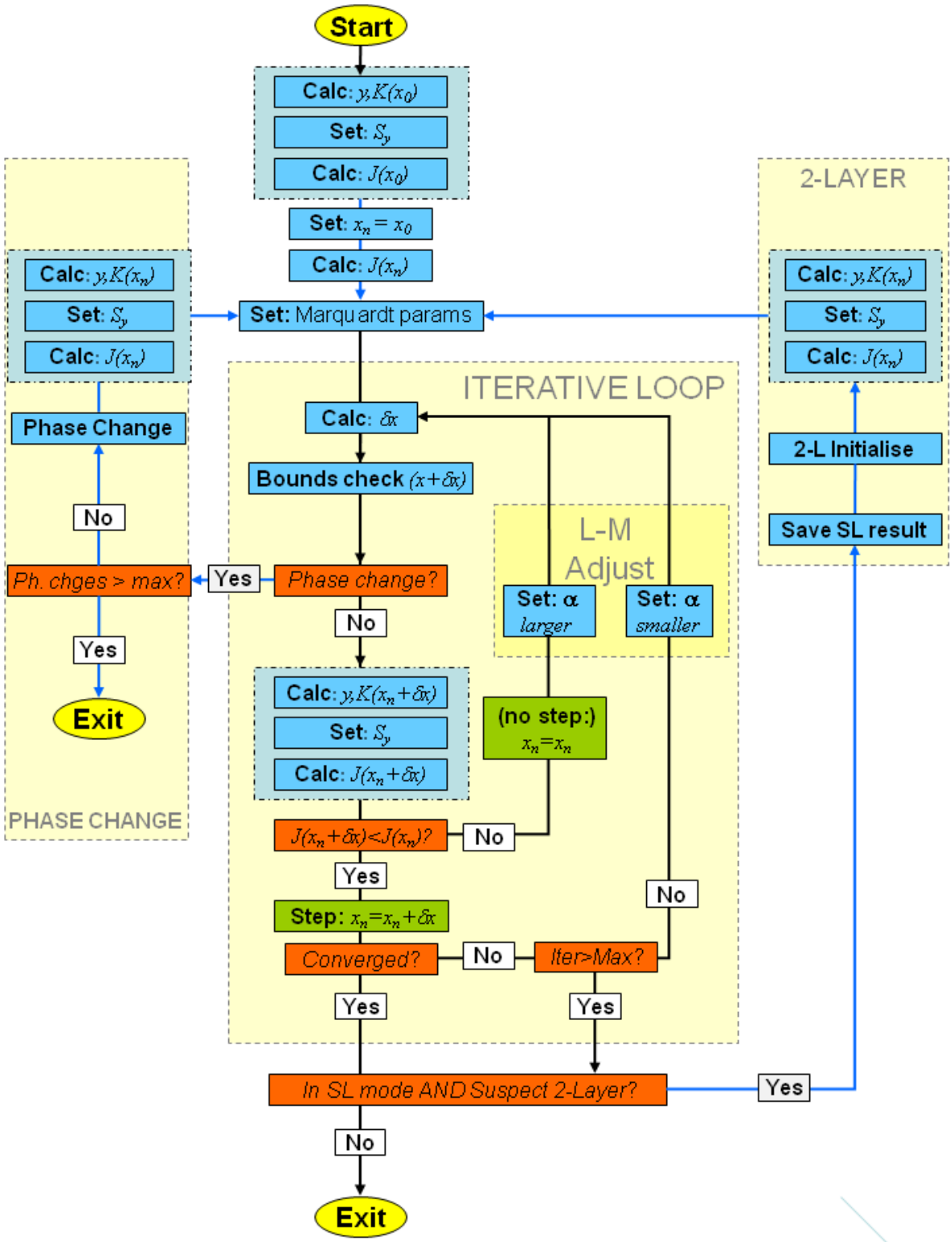

Figure 5: Flow diagram of the Levenberg-Marquardt algorithm in OCA

3.5.3 Operational Considerations

In the original ([RD-1]) concept for OCA, full flexibility was given via indexing methods over the inclusion of channels and state variables. This was to allow for

- Removing channels in particular illumination conditions, e.g. 3.9 μm during 'twilight' (low sun but not night-time) when the RT modelling is known to be too difficult,
- Removing state parameters when the overall information available (e.g. night or twilight) is reduced leading to a poorly defined inversion problem and conversion problems.

In practical terms this strategy leads to complicated code with dynamically sized arrays and complex indexing. For the operational implementation of OCA with MSG SEVIRI, the approach has been somewhat different. The full measurement and state vectors are maintained and the availability of channels / parameters determined through setting error covariance values. A **measurement** can be 'removed' by **raising** its' error to a very high level (∞). A **state** parameter is removed by **lowering** its' error to a low level (zero). There are some considerations:

For Measurements - the approach is entirely valid and has the advantage that the channel's fit to the retrieval is monitored even though it does not influence the result. This can lead to a learning process that can later lead to improved modelling and the channels' inclusion. The disadvantage is the extra cost of the RT for the channel and the matrix algebra that continues to work on full size matrices. The RT can be sensibly avoided where there is clearly no benefit in monitoring (e.g. solar channels at night), but the extra algebraic cost is unavoidable.

For State parameters - reducing the scope of the problem in reaction to the information available is not particularly sound as such; however the disabled state parameters can take on the role of fixed model parameters and their effect be accounted for as given above either through equation 36 (post retrieval accounting) or equation 38 (EQMPN, in retrieval accounting). The EQMPN method might be expected to return the problem to its' ill-posed nature and so, pending more research and experience (on especially night-time retrievals) the post retrieval error accounting it to be preferred.

3.6 Output Description

In addition to the cloud products the OCA method permits a wealth of ancillary information based on the error analysis and cost and cost-related measures. The following table displays all possible outputs indicating those likely to be of practical interest to users of the products and therefore constituting the OCA output, and those additional diagnostic parameters of interest to algorithm developers.

				Associated variables				
Parameter	**Description**	**units**	**Dim**	**Value**	**Error**	**FG**	**AP**	**availability**
OCA Model	Flag to indicate cloud model used Discrete values for: **NC**-No cloud; **SLW**-single layer water; **SLI**-single layer ice; **2L**-2-layer ; **SLD** –single layer dust; **2LD** – 2-layer dust; **SLA** – single layer ash; **2LA** – 2-layer ash	none	1	✓	×	×	×	NC,SLW, SLI, 2L
COT layer-1	Optical thickness of uppermost cloud layer	none	1	✓	✓	☑	☑	SLW, SLI, 2L, SLD, 2LD, SLA, 2LA
CRE layer-1	Effective radius of uppermost cloud layer	μm	1	✓	✓	☑	☑	SLW, SLI, 2L, SLD, 2LD, SLA, 2LA
CTP layer-1	Top pressure of uppermost cloud layer	hPa	1	✓	✓	☑	☑	SLW, SLI, 2L, SLD, 2LD, SLA, 2LA
CFR layer-1	Fractional coverage of uppermost cloud layer	none	1	✓	✓	☑	☑	SLW, SLI, 2L, SLD, 2LD, SLA, 2LA
TS	Skin temperature	K	1	✓	✓	☑	☑	SLW, SLI
COT layer-2	Optical thickness of lower cloud layer	none	1	✓	✓	☑	☑	2L, 2LD, 2LA
CRE layer-2	Effective radius of lower cloud layer	μm	1	✓	✓	☑	☑	2L, 2LD, 2LA
CTP layer-2	Top pressure of lower cloud layer	hPa	1	✓	✓	☑	☑	2L, 2LD, 2LA
CFR layer-2	Fractional coverage of lower cloud layer	none	1	✓	✓	☑	☑	2L, 2LD, 2LA
S_x	State parameter posterior error covariance	mix	5x5	☑	×	×	×	SLW, SLI, 2L, SLD, 2LD, SLA, 2LA
Jm	Measurement cost	none	1	✓	×	×	×	SLW, SLI, 2L, SLD, 2LD, SLA, 2LA
JmIR	Infra-red measurement cost	none	1	✓	×	×	×	SLW, SLI, 2L, SLD, 2LD, SLA, 2LA
Ja	A priori cost	none	1	✓	×	×	×	SLW, SLI, 2L, SLD, 2LD, SLA, 2LA
dY	Measurement residuals	none/ K	16	☑	×	×	×	SLW, SLI, 2L, SLD, 2LD, SLA, 2LA
Iter	Iteration count	none	1	☑	×	×	×	SLW, SLI, 2L, SLD, 2LD, SLA, 2LA
M	Ash Mass Loading (only for ash layers)	gm^{-2}	1	M	N	N	N	SLA, 2LA

Table 7 output parameters. *Key: ✓- available: user-type output ☑-available: extended diagnostics output, × - not available.*

4 Implications of new FCI channels and characteristics

This section discusses some of the implications of the new channels and altered (current) channel characteristics for the OCA algorithm. As impacts have not to date been formally studied, the comments here are to varying degrees speculative and some areas will require study, either pre or post-launch. We have tried to indicate the degree to which questions remain open.

4.1 Additional Channels

4.1.1 2.2 micron

This is similar to the 1.6 micron channel in particle size response but with greater particulate absorption and therefore less penetration into the cloud. It has however no similar phase (water/ice dependency). What is not understood to date is the degree of extra information that the channel brings; whether the OCA cloud model needs or should incorporate a particle size vertical gradient or the differences to the 1.6 and 3.8 micron channel response need only to be absorbed into by means of a model parameter noise to reflect the incomplete physics. MODIS (which carries 1.6, 2.2 and 3.8 channels) level 2 products include several particle size retrievals obtained from the channels separately, but if we are to follow the principles of the OCA method, an attempt would be made to incorporate the physical effects into a single cloud model.

4.1.2 0.96 micron

This is an entirely new channel in the context of the OCA algorithm. It is responsive to (total) water vapour above the cloud. It can be expected to give some information on CTP, or on above cloud humidity depending on the prior accuracy of the humidity. Experience with SEVIRI has demonstrated that the *infrared* water vapour channels are useful, particularly in the context of solving for two-layer CTPs (see section 7.1), and the new 0.96 micron channel may be expected to be similarly useful (albeit daytime restricted) with the advantage that, given that there is no thermal emission at this wavelength, only the accuracy of the total column water above cloud is a issue in its interpretation, not the vertical distribution.

4.1.3 1.38 micron

This is also an entirely new channel and, in the OCA context, with similar possibilities and limitations (daylight only) as the 0.96 micron channel. It has, compared to the 0.96 micron, a stronger response to water vapour above the cloud and thus could well add to rather than merely duplicate this channel's information. We expect that much stronger constraints on two-layer system CTPs will be available with the availability of these new shortwave channels.

4.1.4 0.44, 0.5 microns

These channels are predominantly intended for aerosol quantification, and in the context of OCA cloud might be envisaged to aid quantifying the aerosol in cloudy pixels (mostly above

cloud aerosol therefore). Also, again because of the strong aerosol and molecular scattering, these channels will have a significantly different response to sub-pixel cloud fraction to the 0.6 and 0.8 micron visible channels and therefore may strengthen the available information on cloud fraction. Of course the proviso is that the aerosol effect can be sufficiently well modelled or proxied.

4.2 Altered Channels

Several channels with SEVIRI heritage are somewhat altered in their spectral response compared to SEVIRI. As these changes are minor and designed to reduce the atmospheric absorption compared to the SEVIRI equivalents, there are no significant science changes implied, and we expect overall more accurate modelling and greater information extraction from the channels.

4.2.1 0.86 micron

The MTG FCI version of this channel is shifted, compared to SEVIRI, to a longer wavelength to avoid contamination by moderately strong water vapour lines. In the context of OCA the clear atmospheric parts of the fast RT should automatically cope with the changed channel location (i.e. currently pre-calculated transmittances will be higher than for SEVIRI 0.81 microns).

4.2.2 1.61 micron

Compared to MSG SEVIRI the FCI 1.6 micron channel is at slightly shorter wavelength and significantly narrower. This is intended to avoid water vapour contamination in the SEVIRI 1.64 micron version. As with the 0.8 micron channel the RT for this channel is automatically updated here including possible just-significant changes to the cloud LUTs because of altered particle size response.

4.2.3 3.8 micron

Compared to MSG SEVIRI the 3.8 micron channel is at a shorter wavelength and somewhat narrower. This is intended to avoid serious CO2 contamination in the SEVIRI 3.9 micron version. As with the 0.86 and 1.61 micron channels the RT for this channel is automatically updated but here there are possibly small changes to the cloud LUTs because of altered particle size response.

4.3 High Spatial Resolution

FCI shortwave channels with 1 Km and 500 m ground ifovs (Table 1) will mean that of 3D radiative transfer effect will be more apparent (especially for non-absorbing shortwave channels) than for the current SEVIRI (~3Km channel size). Effects are expected to be relatively small but will be greater with the 500 m channels and may easily be large enough to impact fit qualities (costs) and therefore of course product quality within OCA unless attempts are made to model such effects in the LUTs. This would be a substantially new area to research and make progress although considerable experience is available within the wider

community e.g. through the Eumetsat Fellowship with DLR (ending 2011). A somewhat unsatisfactory but nonetheless available fall-back position in case of large problems with 3D RT would be simple averaging of radiances back to SEVIRI-like ifovs.

4.4 IRS sounder

The potential availability of hyperspectral sounder (IRS) information, albeit from a IRS scan of order 30 minutes previously, may provide complementary information to aid the OCA product extraction. Useful information would most likely be from a) more accurate (than NWP) T, Q and O profiles enabling improved clear atmosphere radiance terms (see 3.5.1.4 and 3.5.1.5) and b) complementary information on cloud layer(s). Cloud information from IRS should be of high quality because of the large number of 'CO_2' channels available. It's use for OCA and FCI would be somewhat compromised by sampling issues and inherent resolution differences, but it could nevertheless provide important first guess or prior information.

5 PRODUCT CHARACTERISTICS

This section illustrates OCA outputs from MSG SEVIRI as examples for guidance. It is based on single layer only retrievals and therefore does not completely represent the current state with the additional 2-layer functionality. The processed area is shown in Figure 6 as a true colour composite from the 0.6, 0.8 and 1.6 µm channels. The scene contains land and sea pixels, vegetated and desert surfaces, semi-transparent and thick cirrus, cumulus and stratiform low clouds.

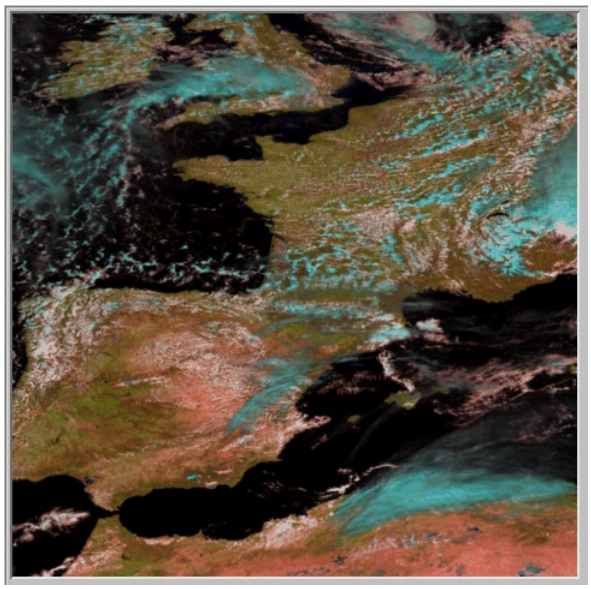

Figure 6: SEVIRI sample OCA processing area

The following sections give some of the characteristics of the OCA output as general guidance. It is not meant as an exhaustive description.

5.1 Diagnostics: Measurement Cost, Iterations and Residuals

The iterations count for the test area is shown in Figure 7; as an image centre and as a histogram to the right. The true colour image is repeated left for reference.

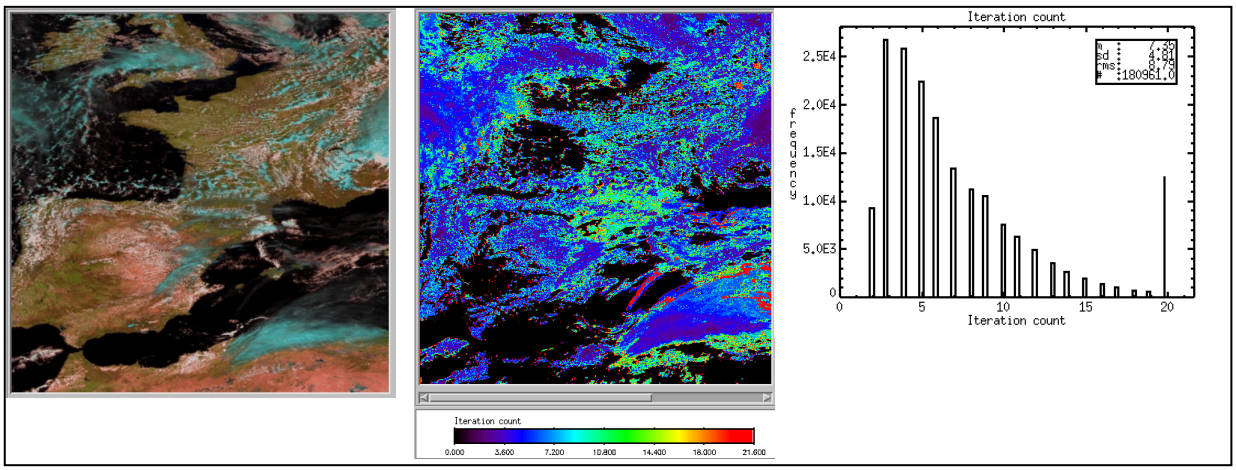

Figure 7: Iterations

Low iteration counts (dark blues, 1-5 iterations) are found generally in the homogeneous and thicker cloud areas, both water (e.g. central Spain) and ice (e.g. N. Africa, central UK). High iteration counts are found for thinner clouds and broken cloud fields. The histogram shows a typical form: average values between 4-8, a peak at 2-4 and a long decreasing tail of high values. The peak at 20 iterations is due to the limit imposed in this run. The peak values can be seen (red in image) to be related to very thin cirrus in the Mediterranean although it is not clear why low counts are found immediately adjacent to peak values.

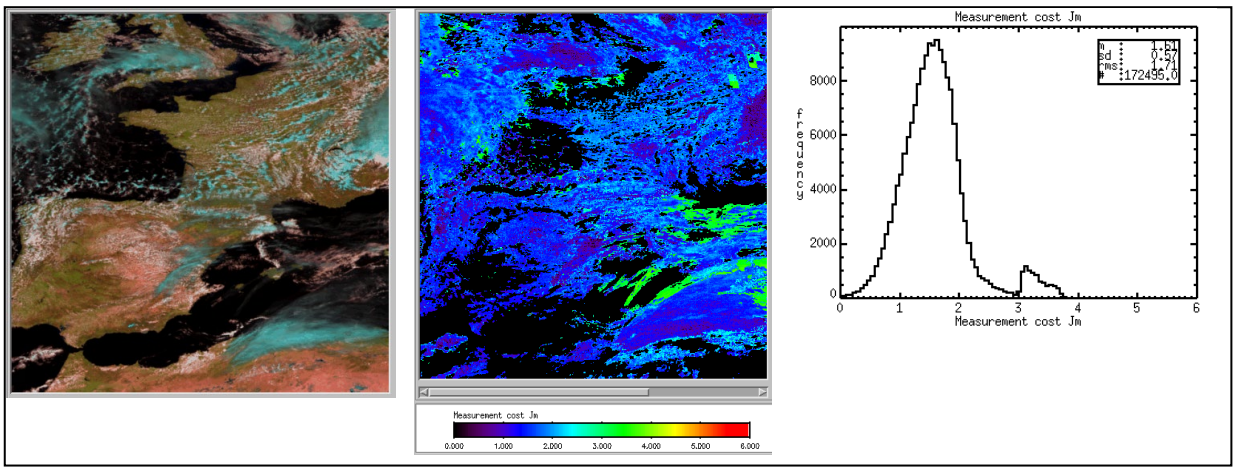

Figure 8: (Log_{10}) Measurement Cost

The measurement cost, J_m, Figure 8, is seen to follow a similar pattern as the iterations with lower values in the homogeneous thicker clouds. Although not particularly clear from these images, the cost is also raised over mixed layer clouds; see the cirrus over cumulus in the Western Approaches of the UK and over where Denmark would be if visible. The histogram shows a typical peak value of Log_{10} J_m ~1.5 (J_m ~30) but the shape is slightly unusual in the secondary peak between 3 and 4 (1000-10000). These very high costs are in the same thin cirrus areas as the high iterations were noted and might warrant further investigation. Note the mean cost *per degree of freedom* is around $30/12 \approx 3$ [22], which suggests noise levels in the channels are set too low. Discussion in section 3.5.1 has described the difficulty in assigning error values to the measurements and this is reflected here in that some degree of empiricism is required in determining what is acceptable as a solution cost. With the setup (channels, errors etc.) used in the OCA implementation used here, a J_m threshold of ~ 90 (Log_{10} J_m ~1.95) has been established as a suitable cut-off value (see section 6).

[22] the number of degrees of freedom in the system is the number of active channels plus state parameters

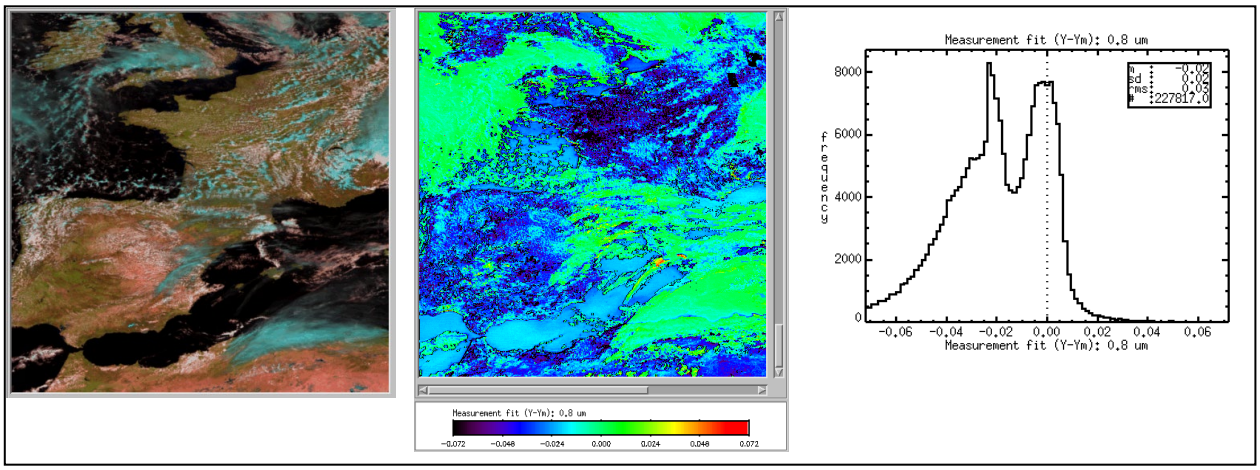

Figure 9: Residual - 0.8 μm channel, fractional reflectance

Figure 9 shows the residual, $y(\hat{x}) - y_m$, in the 0.8 μm channel. It shows that for cloudy pixels the residual is acceptably small (the part of the histogram centred over 0.0 is from clouds). Certainly there are no high residuals corresponding to the very high cost regions noted above. Examination of residuals in the IR channels (not shown) show that it is in these channels that the problem lies.

Residuals are also shown for the cloud free pixels. Here there is no OCA minimisation[23] but the calculated cloud-free reflectance is compared to the measurement. The peak value around -0.02 corresponds to the ocean areas and shows there is a systematic albeit not too large error here. Land pixels show greater deviations up to more than -0.06 especially over northern France. This could be the cause of the somewhat higher costs in this region in Figure 8. Such monitoring of the clear pixels is very useful for checking the quality of the ancillary data and RT models.

5.2 Cloud Phase

In Figure 10 we sow the first guess and final cloud phase determination. Cloud free pixels appear as orange, liquid water cloud as cyan and ice as green. The clear difference is the much higher ice phase coverage in the final evaluation which appears to correspond more closely with the subjective interpretation of the true colour image where, traditionally, ice phase cloud appears in the cyan colour. An incorrect first guess value is in itself no problem but it might be that an improvement would lead to fewer iterations and therefore running costs. From this evidence, the first guess phase procedure (section 3.5.1.7) might be reviewed.

[23] and therefore of course no attempt to reduce the residual as in the cloudy pixel case

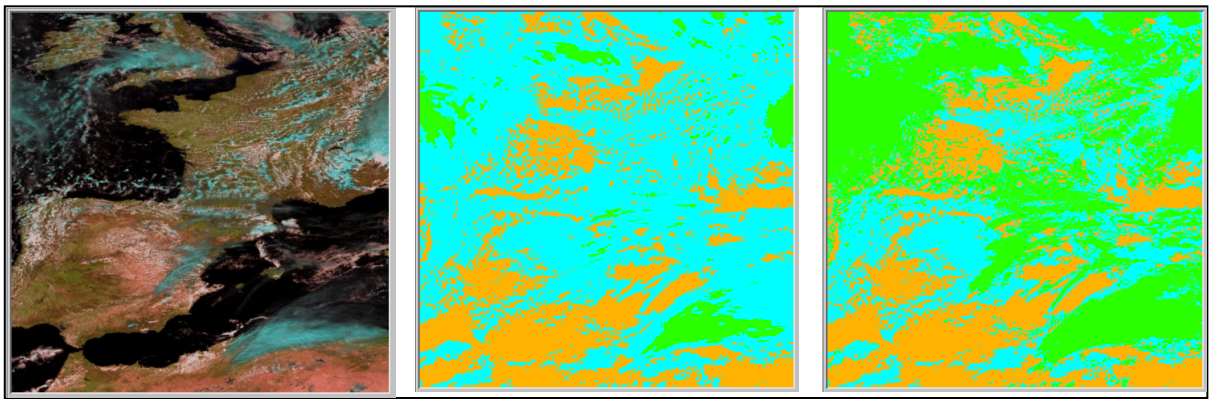

Figure 10: First guess (Centre) and Retrieved phase (Right)

5.3 COT

Retrieved COT is shown in Figure 11. Normally there should be a direct comparison to the visible channel brightness; in the true colour image the presence of the 1.6 μm channel with higher absorption hides this. The histogram is usually more useful for spotting anomalies in COT. In this case we can see discontinuities at the LUT discretisation values and a collection of very high values (=256, LUT limit). It is not known what causes the discontinuities but they are probably related to weak minimisation gradients near the solution, the convergence criteria and linear LUT interpolation methods.

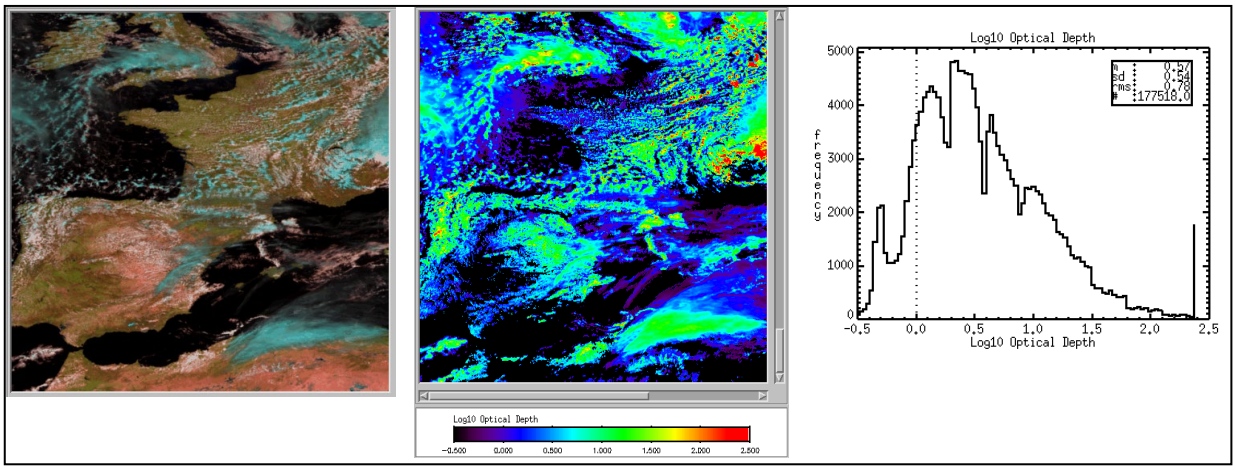

Figure 11: Log_{10} Cloud Optical Thickness

5.4 CRE

The retrieved cloud effective radius also shows some LUT table effects for probably the same reasons. The histogram is appears to consist of two parts here and effectively less than 23 μm constitutes liquid phase cloud and greater than 23 μm, ice phase. Actually the ice LUTs used in these results include CREs to as low as 10 μm and the histograms technically overlap; the CPHS output parameter should be used to determine phase.

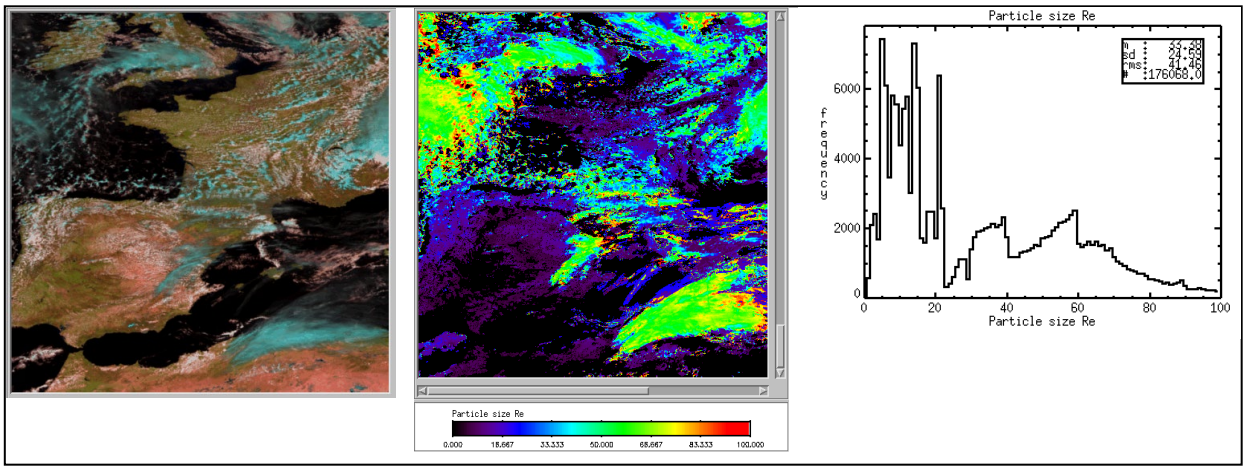

Figure 12: Cloud effective radius, microns

5.5 CTP

Figure 13 shows the retrieved CTP and the estimated error in the CTP. The error is strongly related to the cloud optical thickness and the thin cirrus areas that gave high iteration counts and costs, also have high expected errors.

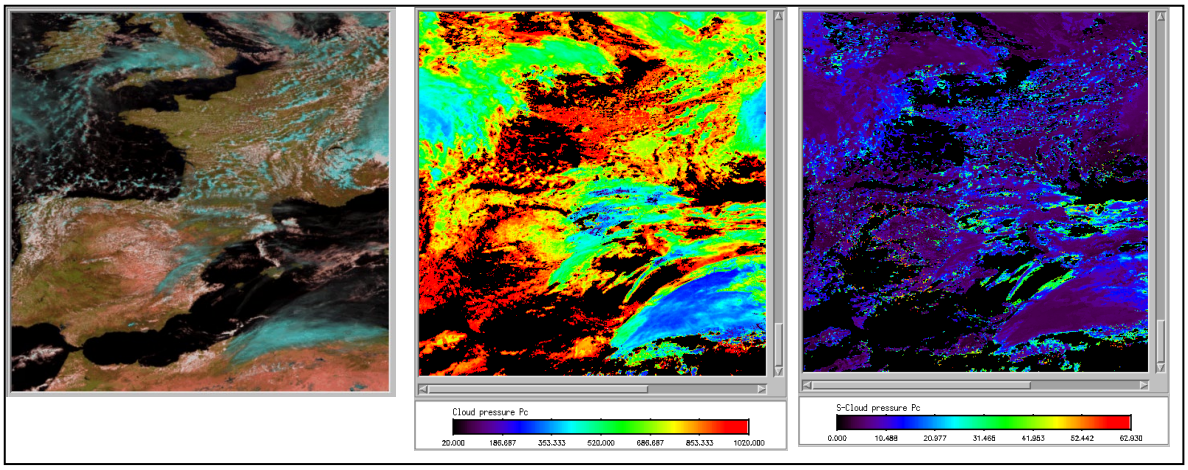

Figure 13: Cloud top pressure, hPa

An effective use of the quality control information is clearly seen in the cirrus area over North Africa in Figure 14. Images and histograms of the retrieved CTP are shown successively top to bottom with no pixels removed, with pixels with expected CTP error > 20 hPa removed and then additionally with pixels with J_m cost > 50 removed. The elimination of the presumed erroneous mid-level CTPs can be seen.

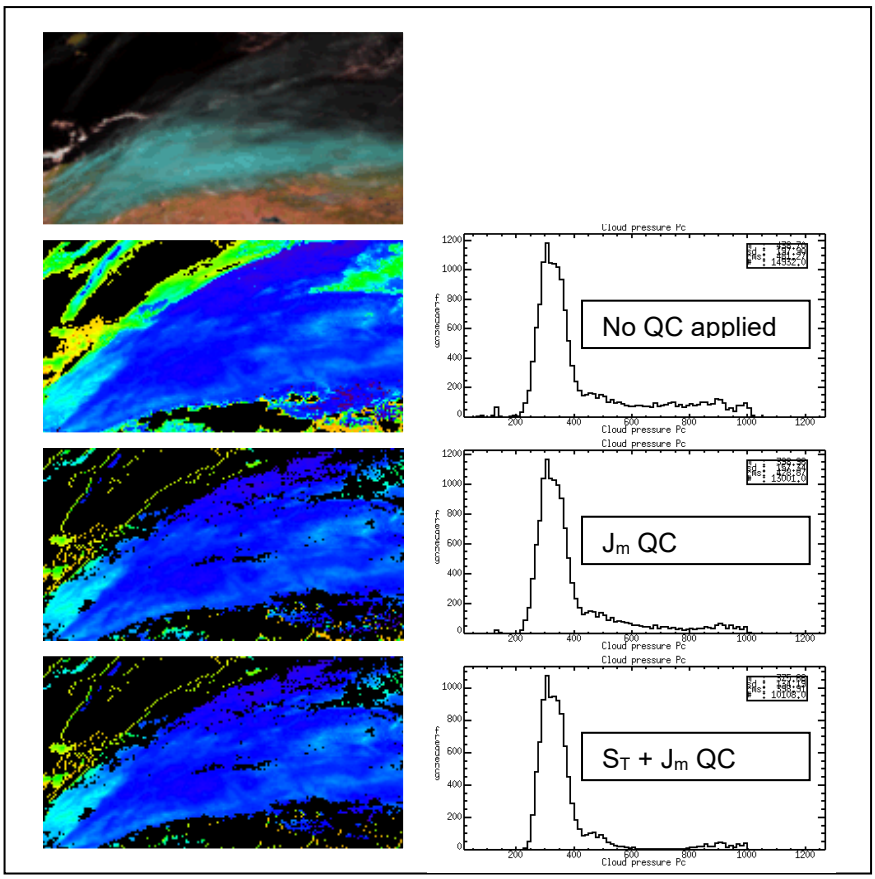

Figure 14: Effect of QC on CTP retrievals

6 PRODUCT VALIDATION

Whilst cloud products are relatively difficult to validate, in recent years the advent of the A-Train satellites with microwave, active lidar and radar has enabled a good quantification of the accuracy of the SEVIRI OCA products. What is presented here is not a thorough validation exercise but intends to characterise the expected accuracy of the products and highlight weak points and strengths of the method. The discussion relates to daytime operation of OCA; the characteristics of IR-only operation at night are not yet fully documented. It also refers to pixels classed as single layer (as determined by the scheme itself) except where 2-layer results are specifically identified.

6.1 COT compared to MODIS

OCA COT values are found compare well to those from the MODIS instrument although this result was only obtained following a calibration adjustment to the 0.6 and 0.8 µm channels. This adjustment was made in response to independent assessments by various researchers that these channels were under-calibrated by around 6-8%. The assessments were mostly made by comparison to collocated MODIS reflectances so the improved agreement to MODIS COT was not really surprising. Nevertheless, the results shown in Figure 15 are reassuring. The data used, as can be seen from the image strip top, is from an area of stratocumulus where collocation and geometrical differences between the two instruments would be minimised. The dotted line in the image shows the nominal A-Train sub-satellite track from which the data are taken.

A more independent albeit indirect test of the OCA COT results is available from comparisons of liquid water path (LWP) with AMSR data (section 6.3).

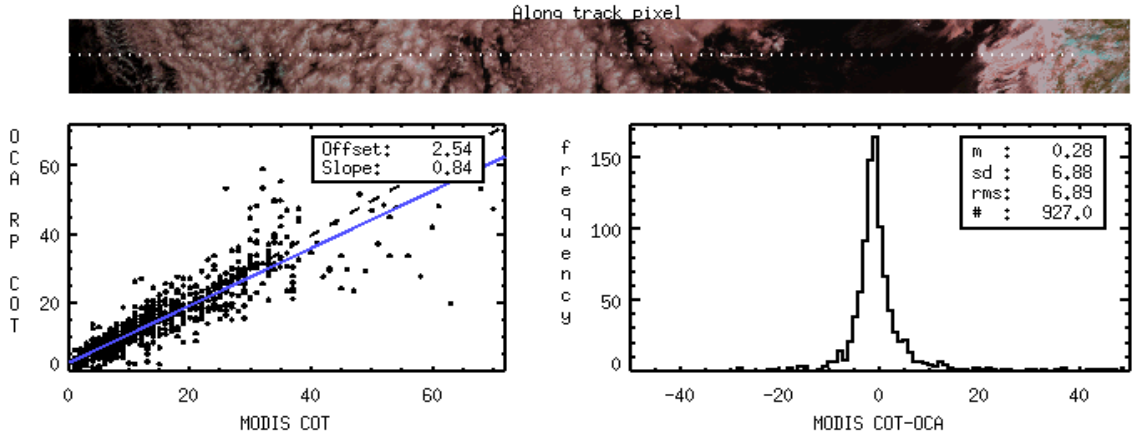

Figure 15: Comparison of OCA and MODIS COT. Blue line shows fit to data.

6.2 CRE compared to MODIS

Again the only real validation option from the A-Train data is with MODIS and again the agreement found is only satisfactory when the calibrations of the 0.6 and 0.8 µm channels are adjusted.

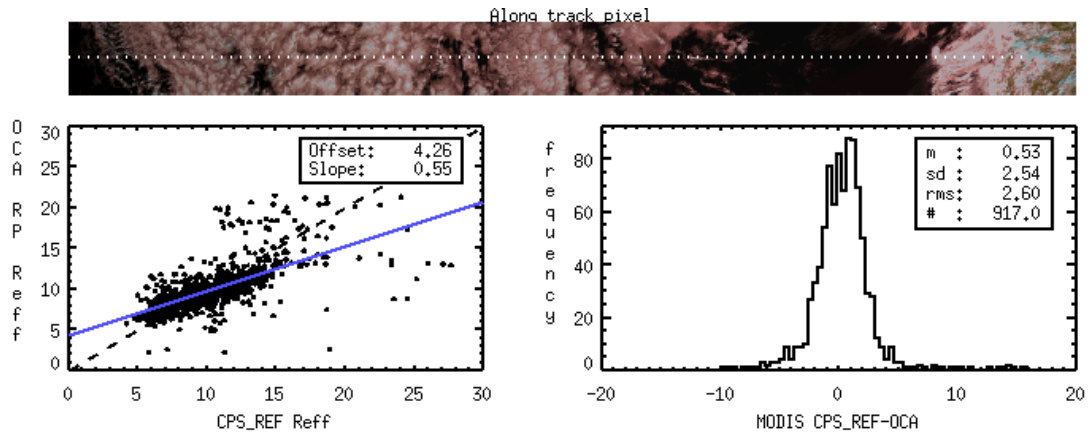

Figure 16: Comparison of OCA and MODIS CRE

Over the same area as for the COT comparison, the CREs from MODIS and SEVIRI-OCA agree to within ~0.5 μm in the mean and ~2.5 μm in standard deviation. The OCA results show less variability than the MODIS in that the line of fit is significantly less than 1:1. It could be that this is related to the different sampling scales of the instruments (~1Km *cf* ~5Km).

6.3 LWP compared to AMSR

As mentioned, a more independent validation of cloud microphysical properties is provided by LWP estimates from the AMSR-e microwave instrument. OCA LWP is generated from the COT and CRE values according to the adiabatic formula which is only valid in non-precipitating stratiform clouds

$$LWP = \frac{5}{9}\tau r_e \tag{39}$$

Figure 17 shows that reasonable agreement is found over stratocumulus. In the A-Train transect shown, the cloud on the right hand side (North, over West African coast) gives poorer agreement with AMSR LWPs around ~50% higher than the OCA values. Probably in this area the cloud is precipitating.

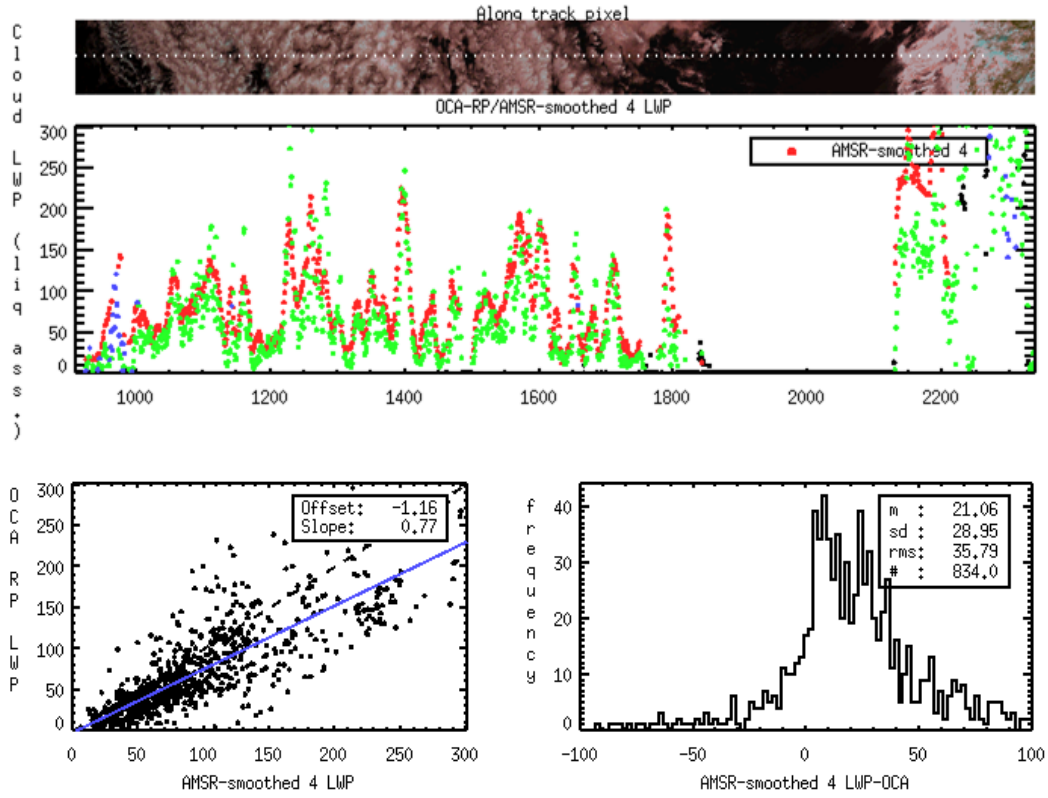

Figure 17: Comparison of OCA and AMSR LWP

6.4 CTP compared to CPR and CALIOP

A wealth of information is available on CTP from the active instruments, CPR and CALIOP, on the A-Train. Here we concentrate on the a few major issues: the overall OCA CTP accuracy and its response to the quality control measures available, the effect of multi-layer cloud and the efficacy of the 2-layer approach adopted; the issue of boundary layer inversions and solution adopted.

6.4.1 Accuracy and QC measures

Figure 18 shows a single daytime half orbit of Cloudsat CPR reflectivity (top) with superimposed OCA retrievals (green for water phase, blue for ice). CPR assessed CTPs are shown as white dots. The lower plots show the comparison of the CTPs as a scatter and as a histogram. The central strip image is the true-colour SEVIRI composite on which the CPR track is marked as a dotted line. The OCA results in Figure 18 have no quality control applied. The mean and standard deviation of the difference CPR-OCA are 0.33 and 2.86 Km respectively.

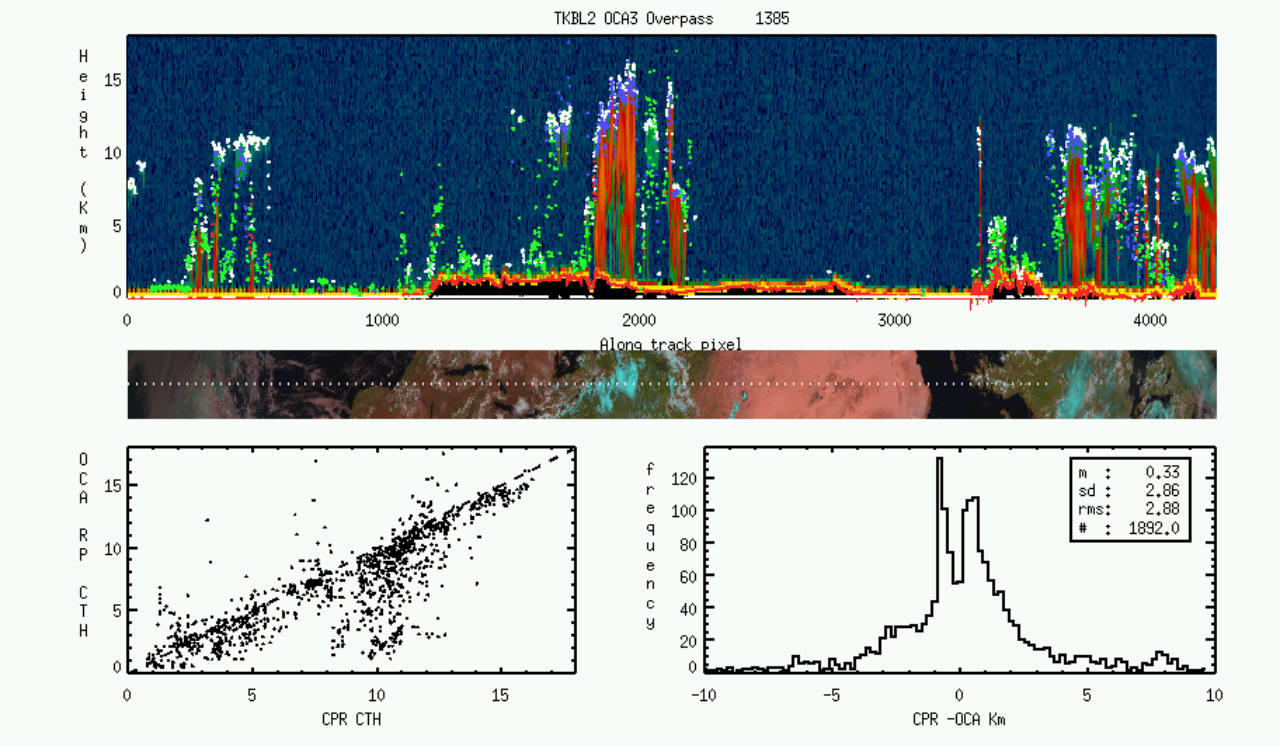

Figure 18: A-Train CPR reflectivity, CTP and OCA CTP compared

The most important QC measure for CTP is the solution cost function. Setting successively tighter thresholds on this quantity leads to continued improvement in accuracy, at the expense of lost data, and is the result of successively eliminating non plane-parallel cloud scenes. For example, Figure 19 shows results from the same case with tighter cost thresholds.

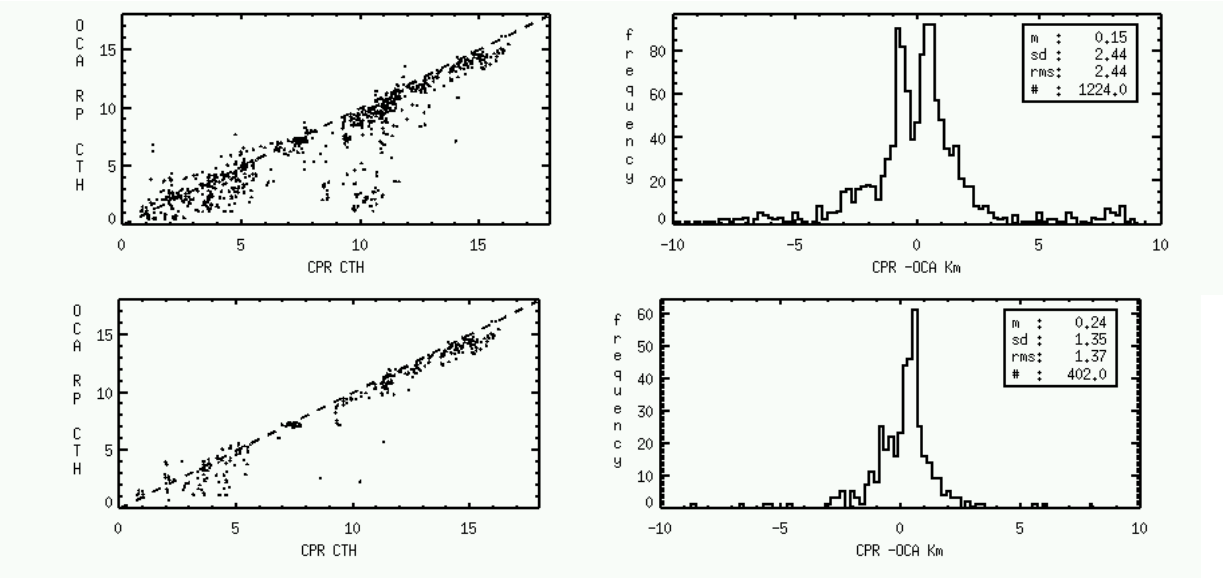

Figure 19: Effect of tightening cost threshold on CTP accuracy

The second quality control measure is the solution expected error, S_T, obtained from equation 33. Applying a threshold on this quantity leads to moderate additional increases in accuracy as judged against the CPR heights. This measure tends to eliminate very thin clouds and clouds at altitudes where the atmosphere is more or less isothermal (e.g. high extended

tropopause). Figure 20 shows a summary of cost and expected error QC on the CTP standard deviation for 17 A-Train orbits. The cyan line, average value ~2.4 Km, is the overall result without any QC applied. The dark blue line is after application of a cost threshold of 90 and shows the largest effect. Smaller reductions are made thresholding the expected CTP error at 10 and 5 hPa (pink and yellow respectively). The gains in accuracy from the error thresholding are obtained however only with the loss of a large fraction of pixels as shown in

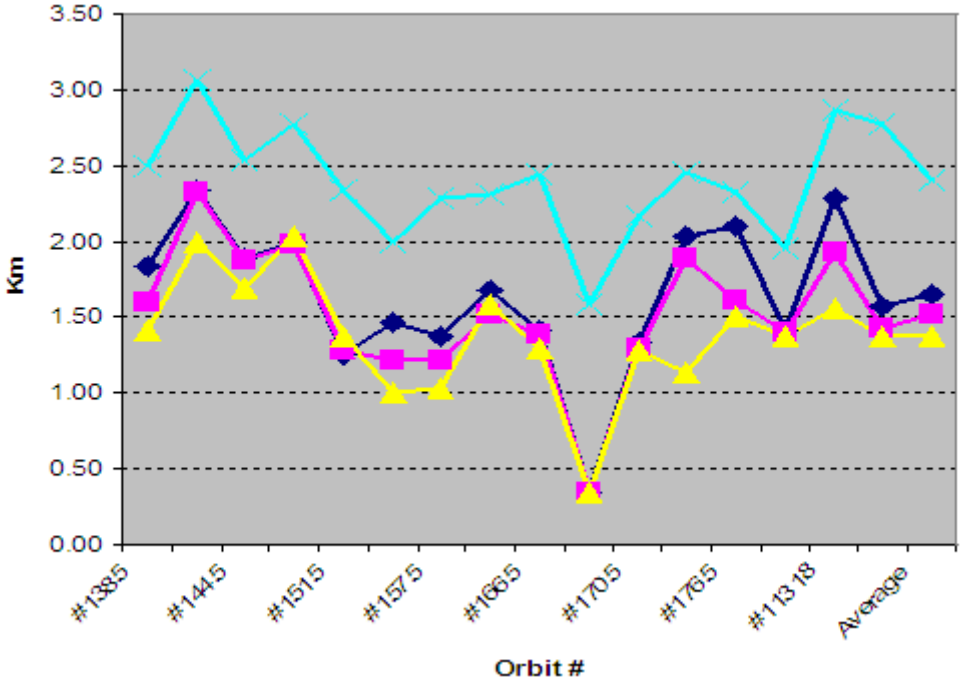

Figure 20: summary of J_m and S_T QC on OCA CTP, 17 ATrain orbits

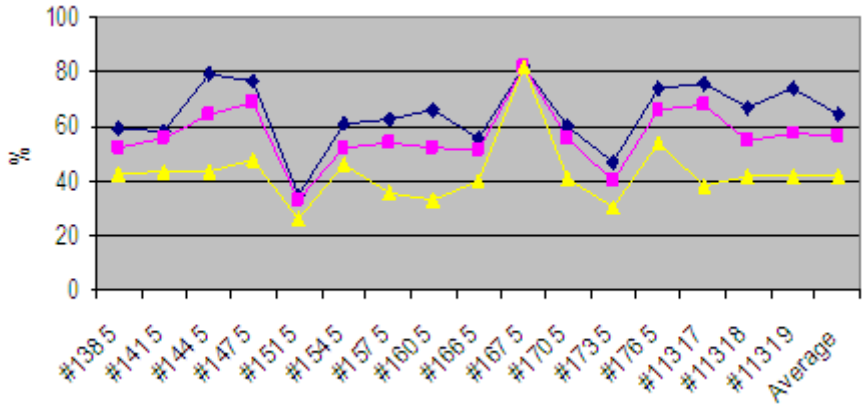

Figure 21: %pixels remaining after QC applications

6.4.2 Multi-layer cloud

Experience from the A-Train CPR and CALIOP reflectivity profiles confirmed what was suspected - that a large proportion of high cost (single layer) OCA retrievals are the result of the presence of more than one layer of cloud. Figure 22 is a typical example from the extra-tropics. In the optically thick 'single layer' cloud at pixels ~2300-2400, the OCA and

MODIS[24] retrievals are in agreement and both around 1-2 Km below the cloud top (as determined by the first CPR echoes). Between 2400 and 2450, two regions of mid and upper level cloud depress the altitude of the OCA CTP (and possibly to a slight degree the MODIS CTP). The red symbols (black on lower plot) show that the OCA cost is high in these cases. From 2470 to 2550 the upper cloud layer is thinner and the MODIS CTPs are now midway between the two layers. The OCA CTPs are mostly at or somewhat above the lower level with a high proportion removed by the cost threshold.

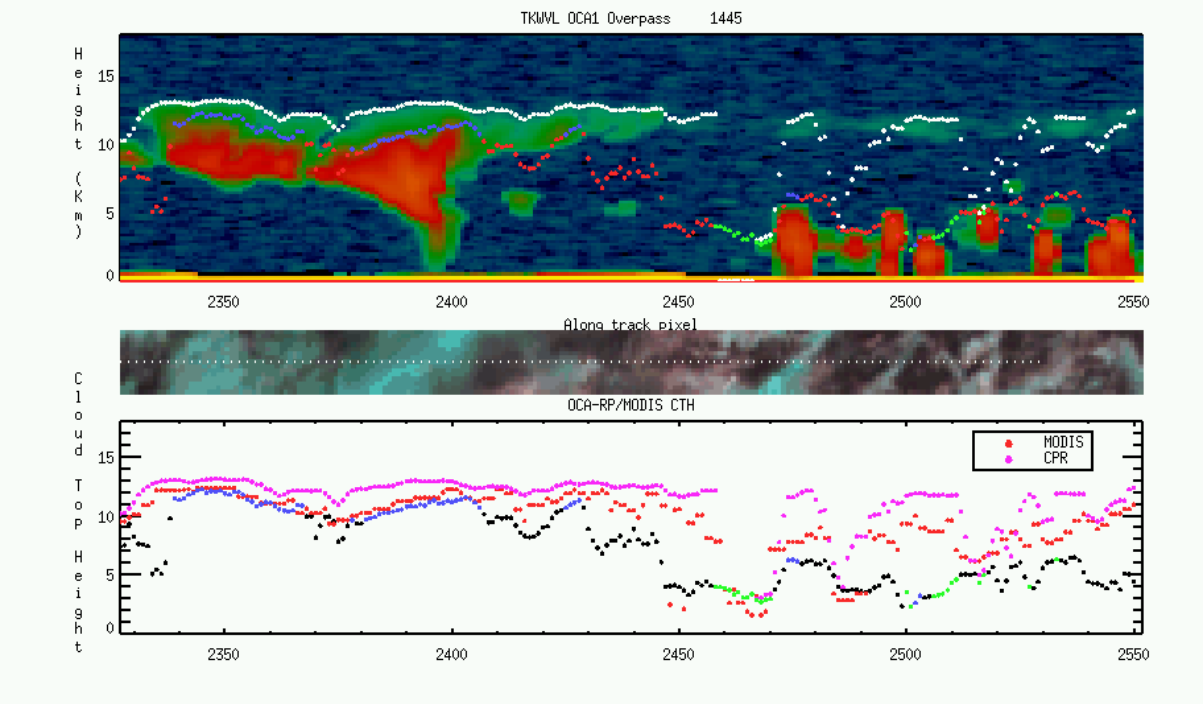

Figure 22: Typical instance of multi-layer cloud. Lower plot shows CTP from CPR (magenta), MODIS (red) and OCA (green-water (low cost), blue - ice (low cost), black - high cost)

The higher sensitivity of OCA to the lower level is because of the use of the VIS channels which 'see' both cloud layers and 'report' a high COT. Fitting the IR channels then requires a relatively low / warm CTP. For the IR-only MODIS result, two layer systems only cause intermediate solutions when the lower layer is moderately high (cold) compared to the surface, otherwise it appears in the IR effectively just like the surface.

Whilst this appears at first sight a major drawback of the OCA method, it is a) easily circumvented and b) offers opportunities.

In the first case, the multi-layer pixels appear to be robustly identified by the solution cost measure. Although good results were obtained using the standard measurement cost (e.g. see RD.3) because this includes high values not caused by multi-layer cloud (e.g. shadowing) it is has subsequently been found that an infra-red channel only cost gives superior results (see section 9.15 for full test description). Once identified as multi-layer the CTP could in principle be recovered by a reprocessing of the pixel with only the IR channels. This would bring results comparable to the MODIS experience, i.e. satisfactory CTPs when the lower level cloud was near-surface but intermediate retrievals for higher lower level cloud. However, a more ambitious approach is taken since the high cost of the multi-layer cases indicates there is more information to be extracted and studies ([RD-2, RD-3] and section

[24] MODIS CTP is based on CO_2 slicing, i.e. an IR-only method.

7.1) show that for some two-layer systems accuracy of the upper layer can be improved dramatically and some information on the lower layer obtained.
A result from the 2-layer retrieval currently employed (see 7.1 for future developments) is shown in Figure 23 for a multi-layer cloud system in the south Atlantic in August 2006, where the background image and white dots are Cloudsat Cloud Profiling Radar reflectances and implied CTH values respectively. The top panel shows the CTH from the standard OCA super-imposed. There are clear deviations towards the altitudes between two layer systems; OCA is especially sensitive to this[25] as it uses VIS and IR simultaneously and therefore 'sees' a high optical depth. The IR channels which effectively determine CTH must work with this high optical depth and consequently place the cloud low in the atmosphere.

In these case though the solution cost is also high and, in the experiment shown in the lower panel, high cost retrievals were re-run using a simple 2-layer model described in this document. The upper layer shows good accuracy with respect to the CPR heights. The lower layer also shows some signs of skill. The upper layer CTH is also quite accurate in the central section where there are no distinct layers and the definition of a lower layer is questionable.
More details on the 2-layer implementation and validation with coincident A-Train data are given in [RD-3].

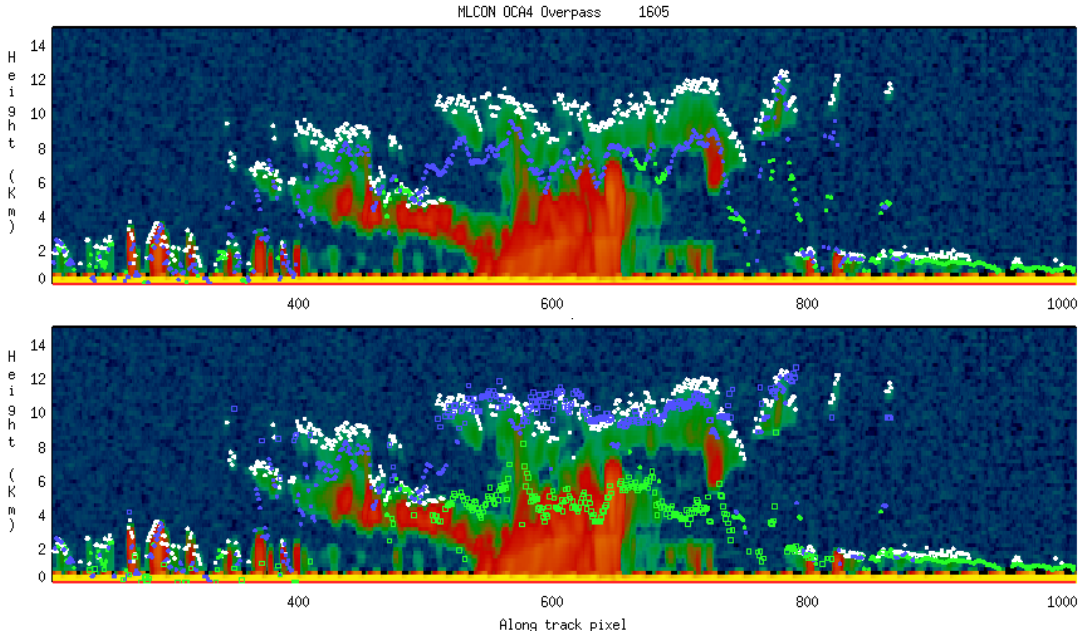

Figure 23: Multi-layer cloud system observed by the Cloudsat Radar 16/08/2006. Top: OCA CTP (blue-ice phase, green-water phase) shown without any quality control filtering. Bottom OCA modified 2-Layer CTPs (blue upper layer, green lower layer).

6.4.3 Boundary layer temperature inversions

These temperature inversions are found in **subsidence** regions and are located in the planetary boundary layer. Cloud, typically stratocumulus, forms in the boundary layer with a

[25] compared to IR-only algorithms. These only have a tendency to error when the lower layer is significantly colder than the surface.

top temperature that is at (and actually partially drives) the temperature of the cold part of the inversion. The 'problem' with such inversions is that with CTPs guess values placed above or below the inversion level, the inversion cannot be 'crossed' by the iterative search to what maybe a the correct solution on the other side. Also, these cases do not typically give rise to high costs since, unlike the tropopause case, the temperature continues downwards again after the inversion as seen in Figure 24 (top right). The figure shows that the same cloud temperature can be obtained both below and above the (NWP determined) inversion. The ambiguity is not necessarily complete since a channel with strong atmospheric absorption could in principle resolve the best of the two solutions. However, the SEVIRI and MTG FCI imagers only have strong absorption in the water vapour channels for which the NWP humidity error adds too much uncertainty to obtain a clear signal. In any case, for the 6.3 µm channel the absorption is too high (such cloud has no effect whether above or below the inversion). The lower panel of the plot shows (red dots) that the MODIS algorithm / sensor is also unable to distinguish between the solutions so that the addition of several CO_2 absorbing channels is also not sufficient with such low cloud. Even in the case of sufficient discriminating channels, any search / minimisation scheme would have to be able to jump the inversion to find the correct solution.

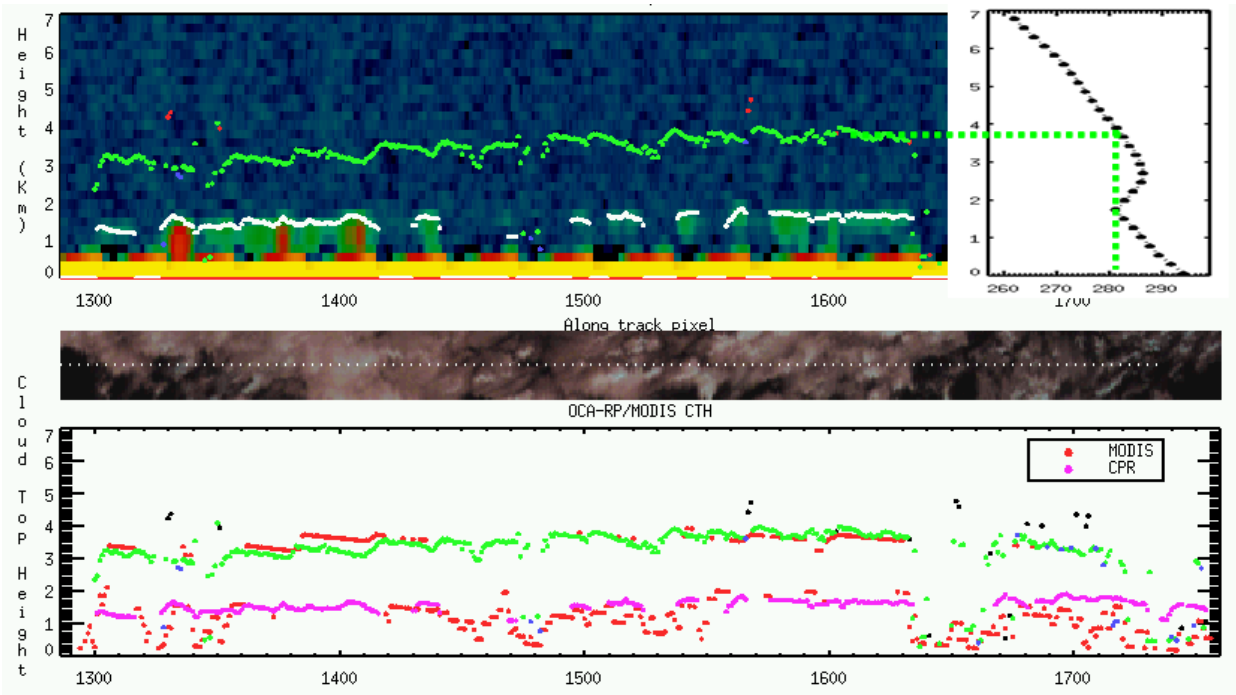

Figure 24: Subsidence inversion effects, NWP temperature profile top right

The solution adopted in OCA is like for the tropopause a physical one: subsidence inversions are detected in the NWP profile and when found, the first guess CTP is placed in the sub-inversion layer and the temperature profile modified to sharpen the inversion, Figure 25 (and see Appendix 8.2 for procedure).

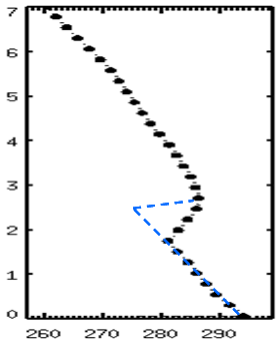

Figure 25: Subsidence inversion modification

Detection is by detecting increasing temperature with altitude in the region up to 702 hPa (RTTOV standard level number 35) and with a corresponding decrease in humidity[26].
The profile 'sharpening' is made because it is thought the smoothed NWP profile may not represent the inversion well. We continue to trust the NWP skin temperature and boundary layer lapse rate. For the case shown in Figure 24, the effect of the change is very positive, Figure 26, with just a few remaining CTP values lying still in the above inversion region. The method appears successful but has not been evaluated for land cases where lower accuracy of the NWP skin temperature and boundary layer lapse rate may cause further problems.

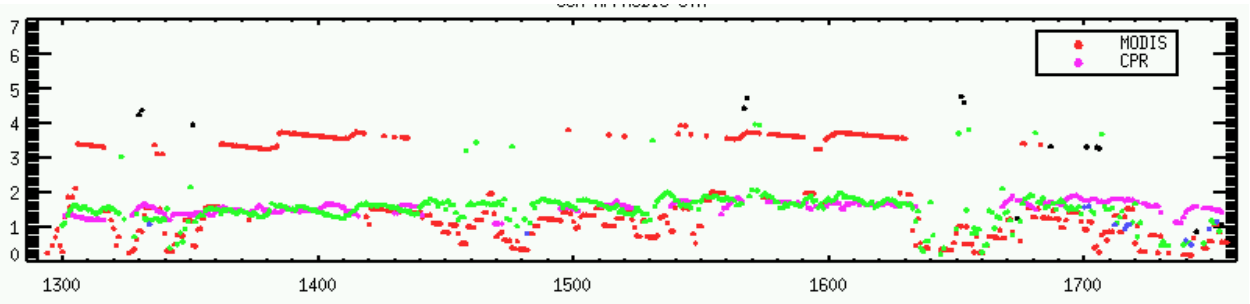

Figure 26: As Figure 24 but after inversion modification technique

[26] This is discriminate subsidence inversions from possible warm front inversions where the cloud top would be expected to be found above the inversion, not below.

7 FUTURE DEVELOPMENTS

7.1 Improved treatment of Multi-Layer Cloud

The 2-layer RT model used in the current implementation (substitution of TS as a proxy lower cloud emitting temperature) is very simplistic and of limited validity:

- it does not allow RT modelling of the solar reflectance channels
- it does not model the transmission of the lower cloud layer[27]
- it does not model correctly the gaseous transmission below or between layers

Despite these seemingly significant drawbacks the results are demonstrably useful (RD.3). However, a fully capable fast RT model for 2 layers developed under [RD-2] should certainly at least match and probably improve upon the IR RT modelling demonstrated here and also permit the use of the solar channels. It is expected that this will be employed within the timeframe of MTG-FCI. In conjunction with the full RT model, the state vector would be expanded to a full 2 layer cloud state: [COT_L, CRE_L, CTP_L, CFR_L, $CPHS_L$, COT_U, CRE_U, CTP_U, CFR_U, $CPHS_U$]. Even with additional channels available compared to SEVIRI, it will be rare that all state vector elements will be significantly constrained by the measurements so that, as now but more so, due attention to the parameter expected errors will be essential.

7.2 Imagery based ancillary data

Currently the only ancillary data drawn from other products of the FCI instrument itself is the cloud mask (SCE) used to determine which pixels to OCA will process. With the potential inclusion of more complex cloud models within OCA (see e.g. section 7.1) or more differentiated models (e.g. distinct cloud types as opposed to merely cloud phases) it is possible that more information from the imaged based scene analysis could be used to guide the OCA model used. A ‘cloud type’ product could for example guide the choice of LUTs used within OCA, and a reliable external estimate of the presence of multi-layer cloud would clearly be useful if OCA where extended to handle two-layer situations.
OCA also relies on NWP forecasted temperature, humidity and ozone estimates at the time of the image in order to determine the cloud-free RT quantities (section 3.4.2.2). Whilst image based products cannot substantially replace the NWP (e.g. the vertical resolution of imagery products is very low), the potential of the imager to provide adjustments at fine spatial and temporal scales is clear. Thus, for example, fields of humidity, skin temperature and ozone obtained from imagery may be used to ‘update’ the NWP-provided background RT information to fine scales. The additional accuracy obtained should translate into improved cloud products obtained from OCA.

[27] Although, as described in this document, reference to the single layer COT result allows for a ‘poor man’s’ estimate of the lower layer transmission *post-hoc*.

8 APPENDIX: IDENTIFICATION AND MODIFICATION OF PROFILE TEMPERATURE INVERSIONS

8.1 Tropopause

Temperature inversions can cause local minima in the cost function and can prevent the correct solution being found. This is not a problem unique to OCA; search methods of many algorithms also get 'stuck' on the wrong side of the inversion. The first was noticed with high cost solutions in the centre of deep tropical convection systems and is the result of **tropopause** overshooting convection

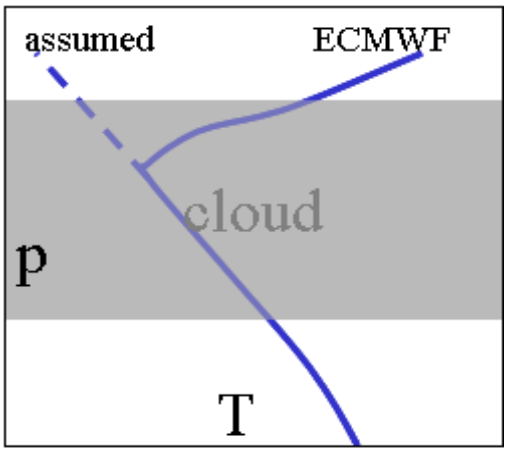

.

Figure 27: Modification to the temperature profile at the tropopause

A cloud that overshoots this ever-present temperature inversion carries on cooling adiabatically and this makes it cooler than the ambient stratospheric atmosphere. The solution to this problem was to identify the tropopause and modify the temperature profile above it to take on the adiabatic lapse rate, **Error! Reference source not found.**. Now the cost function continues decreasing as the CTP in an overshooting case rises above the tropopause. There is no effect on clouds that do not reach the tropopause, so the profile modification is made safely everywhere. It must be noted however that the modification should be made *after* the LW atmospheric RTM calculations are made since otherwise radiant quantities (upwelling, down-welling etc) would be incorrect for clouds that do not reach this level[28].

The identification and correction is achieved by deriving the position (model level) of the tropopause and modifying the temperature profile ABOVE the tropopause to effectively remove the tropopause inversion and replace it with a monotonically decreasing temperature profile with gradient equal to that in the upper layer below the tropopause.

Procedure:

- Search forecast temperature from bottom (higher pressure) upwards for first occurrence of a temperature gradient less than a specific value. Search is to be made between 400 hPa to 85 hPa or nearest appropriate model levels.

[28] and also actually for overshooting optically thin clouds, but as overshooting clouds are inevitably non-transmitting, there is no error induced.

- Temperature gradient defined as $\partial T^i / \partial z = \Delta T^{i,i-1}_{fcst} / 16 \Delta Log_{10} P^{i,i-1}_{fcst}$
- Pressure index i for where $\partial T^i / \partial z < 2.0$ defines the tropopause pressure: $P^{tropopause}_{fcst} = P^i_{fcst}$

- Set forecast temperature profile for pressures lower than tropopause pressure:
  - Calculate below tropopause lapse rate as $\frac{\partial T}{\partial P} = \frac{T^{i+2}_{fcst} - T^i_{fcst}}{P^{i+2}_{fcst} - P^i_{fcst}}$
  - Reset temperatures above: for $j = i - 1 \; to \; 1$ do $T^j_{fcst} = T^i_{fcst} + \partial T / \partial P \left(P^j_{fcst} - P^i_{fcst} \right)$

8.2 Boundary Layer Inversions

Here the forecast temperature profile is checked in the lower layers for a typical anticyclonic temperature Inversion (it should be anticipated that the humidity profile will be subsequently added to make this identification more robust). The profile is modified in the boundary layer to increase its depth in anticipation of model errors and smoothing and allow the subsequent retrieval to find a suitable pressure (analogous to tropopause handling). The procedure primarily affects CTP first guess but note that it is the modified profile and NOT the original profiles that is subsequently used in the retrieval process.

Procedure (see Figure 28):

- Inversion search takers place from bottom up between the forecast model surface level +1 (defining $P^{search\_bot}_{fcst}$) and the RTM model level closest to $P^{search\_top}_{fcst}$.
- An inversion is deemed found if $T^{i+1}_{fcst} > T^i_{fcst}$ (i counting bottom up). This defines and sets a flag INV_BL to true. The following steps only take place if an inversion is found.
- The boundary layer lapse rate, $\partial T / \partial P$, is determined using the two levels below $P^{Inv\_bot}_{fcst}$.
  - $BL_{lapserate} = \left(T^{j+1}_{fcst} - T^j_{fcst} \right) / \left(P^{j+1}_{fcst} - P^j_{fcst} \right)$
  - A search is then made for the 'top' of the inversion feature – this being the point at which lapse rate returns to normal (negative). Thus the top is where $T^{i+1}_{fcst} < T^i_{fcst}$. This search is made from the level index of $P^{Inv\_bot}_{fcst}$ + 2 to force some depth to the feature. This defines $P^{Inv\_top}_{fcst}$.
- The temperature profile is then modified between $P^{Inv\_bot}_{fcst}$ and $P^{Inv\_top}_{fcst}$ replacing the original values with a linear extrapolation in P
  - $T(P_i) = T(P^{inv\_bot}_{fcst}) + BL_{lapserate} \times \left(P_i - P^{inv\_bot}_{fcst} \right)$

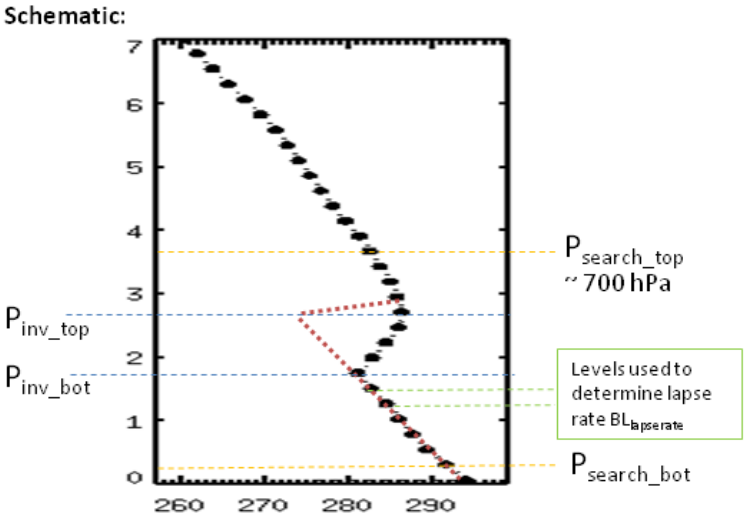

Figure 28 Boundary Layer level definitions

9 APPENDIX: INVERSION FIRST GUESS PROCEDURES

Parameter initialisation, i.e. first guess values, for the initial single layer cloud model attempt by OCA is made so that the iterative procedure of the cost minimisation starts from as close to the final solution as possible and that the AP and Aperrors are appropriately set.
The following table shows the settings made. 'Algorithm' means that the value concerned is derived using an algorithmic procedure as specified later in this section. Sub- and super-scripted symbols are static data; more details and current values of which are provided in Appendix 13.

Model parameter settings for Single layer retrieval				
Variable	FG ($\mathbf{x_o}$)	AP ($\mathbf{x_b}$)	APerror ($\mathbf{S_x}$)	units
CPH	algorithm	n/a	n/a	-
COT	algorithm	$Log_{10}\left(COT_{AP}^{SL}\right)$	COT_{Sx}^{SL}	-
CRE	algorithm	CRE_{AP}^{SL}	CRE_{Sx}^{SL}	microns
CTP	algorithm	CTP_{AP}^{SL}	CTP_{Sx}^{SL}	hPa
CFR	CFR_{FG}^{SL}	CFR_{AP}^{SL}	CFR_{Sx}^{SL}	-
TS	forecast	forecast	$TS_{Sx}(sfc)$	K

As indicated, the 'First Guess' (FG) state parameters are derived using analogous but highly simplified equations of the RTM. The FG parameters are obtained in a strict order as they are not independent procedures. The order (and very brief method overview) is:

- The cloud/no cloud decision comes from the cloud detection dataflow.
- Cloud phase, CPH_{FG}, - day and night: from 8.7-10.8 μm difference providing the cloud detection is not indicating 'dust' or 'ash' in which case this is taken as first guess phase.
- Optical thickness, COT_{FG} – day: 0.8 micron channel with reference to solar-satellite geometry; night: IR channel regression.
- Effective radius, CRE_{FG} – day: from COT_{FG} and 1.6 micron channel with reference to solar-satellite geometry; night: static value based on FG Phase.
- Top pressure, CTP_{FG} – day and night: from COT_{FG}, CRE_{FG} and 10.8 micron channel.

AP and APerrors for all variables are set to Static Data Values appropriate to the input FG phase.

9.1 First Guess Cloud Phase, CPH_{FG}

Cloud phase, i.e. liquid or ice (solid), is the only parameter of the model to have discrete (currently 4) values and if the input scenes analysis does not indicate dust or ash, **CPH_{FG}**, is determined by a threshold check on the 8.7 – 10.8 micron brightness temperature difference;
$if \quad (BT^{8.7} - BT^{10.8}) > -1.2 \quad then \quad iCPH_{FG} = 2 \quad else \quad iCPH_{FG} = 1$
If dust has been flagged then $iCPH_{FG} = 3$ and if ash has been flagged then $iCPH_{FG} = 4$

9.2 First Guess Optical Thickness, COT_{FG}

A. **Daytime:**

Daytime **COT_{FG}** is set using the RBD LUT elements corresponding to **CPH_{FG}** for the 0.67 micron channel.

1. Obtain value of 0.67 reflectance measurement and correct for pixel cloud fractional coverage, CFR_{FG}, only if CFR_{FG} is < 0.95:

$$\rho_{\bullet} = (y_m^{0.67} - (\rho_s^{0.67}(1-CFR))/CFR$$

2. Extract slice of RBD LUT for 0.67 micron channel corresponding to the current first guess phase, observation geometry and class mean effective radius:

$$RBD_{slice} = RBD^{iCPH_{FG}}(0.67,*,i\xi_{sun},i\xi_{sat},i\psi,iR_m^{iCPH_{FG}})$$

Note RBD_{slice} is therefore a vector length equal to the LUT dimension in COT.

3. Adjust slice for surface reflectance:

$$RBD_{slice}^{adj} = RBD_{slice} +$$
$$[(TB^{iCPH_{FG}}(0.67,*,i\xi_{sun},iR_m^{iCPH_{FG}}) + TFBD^{iCPH_{FG}}(0.67,*,i\xi_{sun},iR_m^{iCPH_{FG}})) \times TB^{iCPH_{FG}}(0.67,*,i\xi_{sun},iR_m^{iCPH_{FG}}) \times \rho_s^{0.67}$$
$$[1-\rho_s^{0.67} RFD^{iCPH_{FG}}(0.67,*,iR_m^{iCPH_{FG}})]$$

4. Calculate COT_{FG} from comparison of $\rho_{\bullet}^{0.67}$ with RBD_{slice}^{adj} according to three cases:

   a. If $\rho_{\bullet}^{0.67} < MIN(RBD_{slice}^{adj})$ then $COT_{FG} = MIN(COT_{LUT})$

   b. ELSE If $\rho_{\bullet}^{0.67} > MAX(RBD_{slice}^{adj})$ then $COT_{FG} = MAX(COT_{LUT})$

   c. ELSE COT_{FG} *from Linear _ Interpolate*$(\rho_{\bullet}^{0.67}$ *in* $RBD_{slice}^{adj})$

B: Night time (water or ice phase):

Night time **COT_{FG}** is set using an empirically derived relation to various IR channel brightness temperature values:

$$COT_{FG} = -1.698$$
$$-6.954\times10^{-2}(BT_{10.8} - BT_{12}) + 4.99\times10^{-2}(BT_{6.3} - BT_{10.8})$$
$$-2.264\times10^{-1}(BT_{8.7} - BT_{10.8}) + 1.534\times10^{-2} BT_{10.8}$$

C: Night time (dust phase):

A similar empirical algorithm to B: may be used (not currently defined), but given the low occurrence of dust phase pixels, the (CPU) penalty from using any reasonable value (e.g. the prior value) is not very significant.

D: Night time (ash phase):

A similar empirical algorithm to B: may be used (not currently defined), but given the very low occurrence of ash phase pixels, the (CPU) penalty from using any reasonable value (e.g. the prior value) will be insignificant.

9.3 First Guess Effective Radius, CRE_{FG}

A. **Daytime:**

Daytime **CRE_{FG}** is set using the RBD LUT elements corresponding to **CPH_{FG}** and **COT_{FG}** to the 1.6 micron channel:

1. Obtain value of 1.6 reflectance measurement and correct for pixel cloud fractional coverage, CFR_{FG}, only if CFR_{FG} is < 0.95:

$$\rho_{\bullet}^{1.6} = (y_m^{1.6} - (\rho_s^{1.6}(1-CFR))/CFR$$

2. Extract slices of RBD LUT for 1.6 micron channel corresponding to the current first guess phase, , observation geometry and class mean effective radius and optical thickness LUT values bracketing the first guess optical thickness value:

$$RBD_{slice}^{low} = RBD^{iCPH_{FG}}(1.6, iCOT^{low}, i\xi_{sun}, i\xi_{sat}, i\psi, *)$$
$$RBD_{slice}^{high} = RBD^{iCPH_{FG}}(1.6, iCOT^{high}, i\xi_{sun}, i\xi_{sat}, i\psi, *)$$

Note RBD_{slice} is therefore a vector length equal to the LUT dimension in CRE.

3. Adjust slices for surface reflectance:

$$RBD_{slice}^{low-adj} = RBD_{slice}^{low} +$$
$$[(Tb^{iCPH_{FG}}(1.6, iCOT^{low}, i\xi_{sun}, *) + TFbd^{iCPH_{FG}}1.6, iCOT^{low}, i\xi_{sun}, *)) \times Tb^{iCPH_{FG}}(1.6, iCOT^{low}, i\xi_{sun}, *) \times \rho_s^{1.6}]/$$
$$[1 - \rho_s^{1.6} RFd^{iCPH_{FG}}(1.6, iCOT^{low}, *)]$$

$$RBD_{slice}^{high-adj} = RBD_{slice}^{high} +$$
$$[(TbB^{iCPH_{FG}}(1.6, iCOT^{high}, i\xi_{sun}, *) + TFBD^{iCPH_{FG}}(1.6, iCOT^{high}, i\xi_{sun}, *)) \times TB^{iCPH_{FG}}(1.6, iCOT^{high}, i\xi_{sun}, *) \times \rho_s^{1.6}]/$$
$$[1 - \rho_s^{1.6} RFD^{iCPH_{FG}}(1.6, iCOT^{high}, *)]$$

4. Interpolate slices to COT_{FG} value:

$$RBD_{slice}^{adj} = (COT_{FG} - COT^{low}) \times (RBD_{slice}^{high-adj} - RBD_{slice}^{low-adj}) / \Delta COT_{LUT} + RBD_{slice}^{low-adj}$$

5. Calculate CRE_{FG} from comparison of $\rho_{\bullet}$ with RBD_{slice}^{adj} according to three cases:

   a. If $\rho_{\bullet}^{1.6} < MIN(RBD_{slice}^{adj})$ then $CRE_{FG} = MAX(CRE_{LUT})$

   b. ELSE If $\rho_{\bullet}^{1.6} > MAX(RBD_{slice}^{adj})$ then

   $$CRE_{FG} = CRE_{LUT}(LUT\ index\ of\ MAX(RBD_{slice}^{adj}) + 1)$$

   c. ELSE COT_{FG} *from Lin_Interp*$(\rho_{\bullet}^{1.6}\ in\ RBD_{slice}^{adj})$

B: Night time:

Night time **CRE_{FG}** is set using static pre-defined phase dependent values, **$CRE_{FG}(CPH_{FG})$.**

9.4 First Guess Cloud Top Pressure, CTP_{FG}

CTP_{FG} is set using a transmission corrected 10.8 micron brightness temperature compared to the forecast temperature profile.

1. Transmission correction

   a. ONLY applied if CPH_{FG} is ice (=2)

b. Transmission $\Gamma^{10.8} = TD^{iCPH_{FG}}(10.8, iCOT_{FG}, i\xi_{sat}, iCRE_{FG})$ where

$iCOT = Int[(COT_{FG} - MIN(COT_{LUT})/\Delta COT_{LUT}] + 2$ and
$iCRE = Int[(CRE_{FG} - MIN(CRE_{LUT})/\Delta CRE_{LUT}] + 1$

c. Convert 10.8 micron BT to radiance $L^{10.8} = B(10.8, BT^{10.8})$

d. IF $\Gamma^{10.8} < 0.9$ then correct for transmission (to 'overcast' radiance):

$L_{\bullet}^{10.8} = (L^{10.8} - L_{fcst}^{10.8} \times \Gamma^{10.8})/(1 - \Gamma^{10.8})$ and calculate corresponding 'overcast' brightness temperature $BT_{\bullet}^{10.8}$

e. Check for outlying values:

i. IF $L_{\bullet}^{10.8} < 0$; then **CTP$_{FG}$** is set to static pre-defined phase dependent values.

ii. IF $BT_{\bullet}^{10.8} < T_{fcst}^{tropopause}$ then set $CTP_{FG} = T_{fcst}^{tropopause}$

iii. IF $BT_{\bullet}^{10.8} > T_{fcst}^{level\ n}$ then set $CTP_{FG} = T_{fcst}^{level\ n-1}$

If none of i, ii or iii are met, then the cloud is deemed to lie somewhere within the NWP profile range. The following strategy depending on the presence of a boundary layer inversion then applies.

f. IF $INV_{BL}\ AND\ BT_{\bullet}^{10.8} > T_{fcst}^{P_{inv\_top}}$ then **CTP$_{FG}$** is set by <u>bottom-up</u> (surface up) search and interpolation within the pre-determined inversion levels: $CTP_{FG}\ from\ Lin\_Interp(BT_{\bullet}^{10.8} in\ T_{fcst}\ between\ levels\ n-1\ and\ level(P_{invtop})$

g. IF $NOT\ INV_{BL}$ then **CTP$_{FG}$** is set by <u>top-down</u> search and interpolation between the tropopause level and the surface:
$CTP_{FG}\ from\ Lin\_Interp(BT_{\bullet}^{10.8} in\ T_{fcst}\ between\ levels\ n-1\ and\ level(P_{tropopause})$

9.5 Control and first guess parameters for the Two Layer model

When the inversion step is re-run in the two-layer mode there are no obvious fast algorithms to obtain useful first guess parameters and fixed values can be used.
As the state parameters in this case represent the upper cloud layer, the phase variable CPH is set to ice or dust or ash depending on scenes analysis input. FG, AP and APerror variables are set according to the table in section 9.5 (noting that the values specified are for meteorological cloud cases; values appropriate to dust and ash two-layer situations are still to be determined). It is this particular value setting which effectively defines the two-layer OCA algorithm, particularly the high value to the proxy lower layer temperature prior CTS_{Sx}^{2L} (20K recommended) which permits the appropriate degree of freedom.
As the solar channels cannot be explicitly modelled, measurement error covariance diagonal elements for solar reflectance channels to are set to effectively infinity, S_y (k,k) = 1e+08, k = $0.4 \rightarrow 3.8\ \mu m$ in order to make them passive in the inversion (the solar RT code can also be side-stepped to save CPU load).

APPENDIX: FUNCTIONAL DETAILS OF MARQUARDT INVERSION

The functional descriptions in this Appendix relate to the operations shown in Figure 5.

9.6 Calc: y, K(x)

This operation is the fast RT model and its gradient of **A231**. The **x** vector given is the vector upon which the model is to operate.

9.7 Set: $\mathbf{S_y}$

Sets the value of the error covariance of the measurements. The value is composed of various contributions with static, measurement dependent and state dependent qualities, all of which are assumed channel independent, i.e. the resulting matrix is diagonal. (Static contributions could be set as part of the Measurement Vector Preparation (A13) function.):

Instrument noise as defined by NeR (Noise equivalent radiance) for channels 0.4 – 2.2 μm and NeBT (Noise equivalent brightness temperature) for channels 3.8 – 13.3 μm.

NeR is statically defined for each pure reflectance channel and contributes to the $\mathbf{S_y}$ matrix as $S_y^{NeR,i} = \left(\frac{NeR^i}{f_o^i} \right)^2$ where f_o^i is the (static) solar constant for channel *i*.

NeBT is statically defined for each thermal channel and contributes to the $\mathbf{S_y}$ matrix as $S_y^{NeBT,i} = \left(NeBT^i \right)^2$

Homogeneity and co-registration errors are defined as static fractions of signal for channels 0.4 – 2.2 μm and as static NeBTs for channels 3.8 – 13.3 μm.

For channels 0.4 – 2.2 μm $S_y^{NeHom,i} = \left(NeHom^i \times \rho_{meas}^i \right)^2$ and $S_y^{NeCor,i} = \left(NeCor^i \times \rho_{meas}^i \right)^2$

For channels 6.2 – 13.3 μm $S_y^{NeHom,i} = \left(NeHom^i \right)^2$ and $S_y^{NeCor,i} = \left(NeCor^i \right)^2$

For the 3.8 μm channel includes noise in both solar reflectance and thermal emission parts the noise which must be combined. Thus $S_y^{NeHom,3.8} = \left(\frac{NeHom^{3.8} \times f_o^{3.8}}{\partial L_{meas}^{3.8} / \partial T} \right)^2 + \left(NeHom^i \right)^2$

Surface reflectance model parameter errors are defined through static fractional errors in the surface reflectance value and only apply to pure solar channels 0.4 - 2.2 μm. Thus $S_y^{R_s,i} = \mathbf{K}_{\mathbf{R}s} . \mathbf{S}_{\mathbf{R}s} . \mathbf{K}_{Rs}^T$ where $\mathbf{K}_{\mathbf{R}s}$ is the jacobian *w.r.t.* surface reflectance returned from the RT model A231. Note $\mathbf{S}_{\mathbf{R}s}$ is (currently) defined as diagonal and specified through the variances.

9.8 Calc J(x)

Calculates the value of the cost function at the state **x**.

$$\mathrm{J}(\mathbf{x}) = (\mathbf{y}(\mathbf{x}) - \mathbf{y_m})^T \mathbf{S_y^{-1}} (\mathbf{y}(\mathbf{x}) - \mathbf{y_m}) + (\mathbf{x} - \mathbf{x_b})^{\mathrm{T}} \mathbf{S_x^{-1}} (\mathbf{x} - \mathbf{x_b})$$

9.9 Set Marquardt parameter

The initial value for α is set as a scaled value of the 'average' size of $\mathbf{J''}$ at the first guess state (given by the sum of its diagonals; the trace of $\mathbf{J''}(\mathbf{x_0})$) which indicates the curvature of the cost function. A factor, MQ_{start}, relates the initial value of α to this size; thus: $\alpha_{start} = MQ_{start} \times TRACE(\mathbf{J''}(\mathbf{x_0}))$.

9.10 Calc δx

Calculates the value of incremental step in the state vector $\boldsymbol{\delta x} = -\left(\mathbf{J''} + \alpha \mathbf{I}\right)^{-1} \mathbf{J'}$.

The first derivative of **J** *w.r.t.* **x**, $\mathbf{J'}$, is calculated according to
$\mathbf{J'} = \mathbf{K_x^T S_y^{-1}} (\mathbf{y}(\mathbf{x}) - \mathbf{y_m}) + \mathbf{S_x^{-1}} (\mathbf{x} - \mathbf{x_b})$

The second derivative (which makes the approximation that $\mathbf{K'} = 0_x$) is calculated according to $\mathbf{J''} = \dfrac{\partial^2 \mathrm{J}}{\partial \mathbf{x}^2} = \mathbf{K_x^T S_y^{-1} K_x} + \mathbf{S_x^{-1}}$

9.11 Bounds check

Given a prospective δ**x**, the resulting $\hat{\mathbf{x}} = \mathbf{x} + \delta\mathbf{x}$ is compared to the static limits on all parameters separately. In general, if, for element *k* of the state vector

then $\hat{x}_k = x_k^{lower\_\lim}$

$\hat{x}_k > x_k^{upper\_\lim}$ then $\hat{x}_k = x_k^{upper\_\lim}$

The exceptions to this are for when *k* represents CRE and, in case a. if CPH is ice, in case b. If CPH is water. In these cases a **phase change** is required (other parameters retain values).

The values of limits $x_k^{lower\_\lim}$ and $x_k^{upper\_\lim}$ depend on the parameter and whether the cloud model operating is the single or 2-Layer:

COT: Limits are static and equal to the bounding values of the current LUT.

CRE: Limits are phase dependent and equal to the bounding values of the LUT, but note the phase change qualification described in c.

CTP:

Single layer operation:

IF Daytime AND $\mathrm{Log}_{10}(\tau) < 1.0$ then $x_{CTP}^{lower\_\lim} = P_{fcst}^{tropopause}$

IF Night time AND $\mathrm{Log}_{10}(\tau) < 0.3$ then $x_{CTP}^{lower\_\lim} = P_{fcst}^{tropopause}$

ELSE $x_{CTP}^{lower\_\lim} = P_{fcst}^{tropopause} - \Delta P_{overshoot}$

2-Layer operation:

In all conditions $x_{CTP}^{lower\_\lim} = P_{fcst}^{tropopause} - \Delta P_{overshoot}$

CFR: Limits are static $x_{CFR}^{lower\_\lim} = 0.0$, $x_{CFR}^{upper\_\lim} = 1.0$

TS:

Single layer operation: (TS represents T_{skin})

$$x_{TS}^{lower\_\lim} = T_{fcst}^{skin} - \sigma_{TS} \times \sqrt{S_x^{TS}}$$

$$x_{TS}^{upper\_\lim} = T_{fcst}^{skin} + \sigma_{TS} \times \sqrt{S_x^{TS}}$$

2-Layer operation: (TS represents lower cloud temperature)

$$x_{TS}^{lower\_\lim} = T_{fcst}\left(CTP) + \Delta T_{lower-upper}\right)$$

$$x_{T}^{upper\_\lim} = T_{fcst}^{skin}$$

9.12 Phase change

Change phase variable CPH from current to non-current (e.g. from water to ice)

Set FG CRE to:

$MAX(LUT_{CRE}^{wat}) - 1.0$ if new phase is water or

$MIN(LUT_{CRE}^{ice}) + 1.0$ if new phase is ice.

Set AP and APerror for all variables to Static Data Values appropriate to new phase

Note: FG values for variables other than CRE (i.e. COT, CTP, CFR and TS) should be equal to the output values from the Cost minimisation (A23) at the point the phase change was requested.

9.13 Set α

The control parameter is set smaller or larger according to whether the previous attempted step was respectively successful or unsuccessful. The setting is a simple multiplicative function:

$\alpha = \alpha \times \alpha_{step}$ to set larger,

$\alpha = \alpha / \alpha_{step}$ to set smaller. a_{step} is a static parameter.

9.14 Convergence test

The simple test decides when the LM descent algorithm is no longer providing a significant decrease in cost:

Convergence is confirmed if $abs(J^n - J^{n-1}) < \Delta J^{thresh}$.

9.15 Test 2-Layer (meteorological cloud)

Following the single layer minimisation (either converged or non-converged), the measurement residuals are tested for a significant multi-layer cloud signal:

Multi-layer cloud suspected if

$J^n_{meas\_IR} > \Delta J_{meas\_IR}$ **AND** $(BT^{8.7} - BT^{10.8}) > -1.2$ **AND** $Log_{10}\tau^n > -0.3$ **AND** $Log_{10}\tau^n < 1.54$

Where $J^n_{meas\_IR} = \sum_k \frac{W^k\left(y^k\left(x^n\right) - y^k_{meas}\right)^2}{S_y(k,k)} > \Delta J_{meas\_IR}$, k indexes for all infrared channels (3.8-13.3 μm) and W^k is a channel weight:

for channels 3.8, 8.7, 9.6, 10.8, 12.0 and 13.4 μm $W^k = 1$ in all cases

for channels 6.3 and 7.2 μm $W^k = 1$ where $\left(y^k\left(x^n\right) - y^k_{meas}\right) > 0$ else $W^k = 0$

9.16 Test 2-Layer (dust or ash)

The tests here are still to be determined (both whether they are possible and what form they take) but will likely be of a similar nature.

9.17 Initialise 2-Layer

Set phase variable CPH to ice or dust or ash depending on cloud detection input.

Set FG, AP and APerror variables according to the following table (with empirically determined example values given here for the meteorological 2-layer case, ice above water cloud):

Variable	FG	AP	APerror	Units
COT	$Log_{10}\left(COT^{2L}_{FG}\right) = 0.5$	$Log_{10}\left(COT^{2L}_{AP}\right) = 0.5$	$COT^{2L}_{Sx} = 0.3$	-
CRE	$CRE^{2L}_{FG} = 15$	$CRE^{2L}_{AP} = 15$	$COT^{2L}_{Sx} = 5$	microns
CTP	$P^{tropopause}_{fcst} + \Delta P^{2L}_{FG} = 100$	$P^{tropopause}_{fcst} + \Delta P^{2L}_{FG} = 100$	$CTP^{2L}_{Sx} = 100$	hPa
CFR	$CFR^{2L}_{FG} = 1.0$	$CFR^{2L}_{AP} = 1.0$	$CFR^{2L}_{Sx} = tiny$	-
TS	$T\left(P^{2L-wat}_{fcst} = 800hPa\right)$	$T\left(P^{2L-wat}_{fcst} = 800hPa\right)$	$CTS^{2L}_{Sx} = 20$	K

Set Measurement error covariance diagonal elements for solar reflectance channels to effective infinite, $S_y(k,k) = 10^8, \quad k = 0.4, 3.8\ \mu m$

9.18 Save SL result

All the relevant retrieved variables and diagnostics of the single layer run are saved so that they can be reinstalled as the retrieved quantities if the 2-Layer mode l proves less successful.

10 APPENDIX: MODEL SELECTION AND EXTRACTION OF 2-LAYER PARAMETERS

10.1 Model selection

- If only the single layer model was run, then single layer products and errors are prepared for output.

If the 2-Layer model was run, then the choice of output (saved single layer results or 2-Layer) is made by considering weighted costs of the respective solutions. The weighted costs are $\frac{J_m^{SL}}{J_{norm}^{SL}}$ and $\frac{J_m^{2L}}{J_{norm}^{2L}}$, where J_{norm}^{SL} and J_{norm}^{2L} are expected (or 'normal') costs associated with successful single and 2-layer retrievals respectively. The result with the lowest weighted cost is output. Note that he J_{norm} values for single and 2-layer retrievals will have different values for meteorological (i.e. water/ice) cloud and dust/ash cloud processing.

10.2 2-Layer product and error extraction

In the case of a 2-layer result to be output the retrieved state vector elements are interpreted in terms of the 2-Layer model. The following table shows the mapping from the retrieved (i.e. single layer) model parameters (COT,CRE,CTP,CFR,TS) and their expected errors to the 2-Layer products and errors. A result, COT_{SL}, obtained in the initial single layer minimisation is also used.

2-Layer product Parameter	**Derivation from SL state parameters**	**Note**
COT_{upper}	COT	
Error COT_{upper}	Error COT	
CRE_{upper}	CRE	
Error CRE_{upper}	Error CRE	
CTP_{upper}	CTP	
Error CTP_{upper}	Error CRE	
CFR_{upper}	*Not available (assumed = 1,0)*	
Error CFR_{upper}	*Not available*	
COT_{lower}	From COT and COT_{SL}	See Note i. below
Error COT_{lower}	assumed = Error COT_{SL}	
CRE_{lower}, Error CRE_{lower}	*Not available*	
CTP_{lower}	From TS and COT	See Note ii. below
Error CTP_{lower}	from Error TS	See Note ii. below
CFR_{lower}	*Not available (assumed = 1,0)*	
Error CFR_{lower}	*Not available*	
TS	*Not available*	
Error TS	*Not available*	

Note i. Extraction of COT_{lower}: The previously retrieved single layer value, COT_{SL}, is presumed to represent the sum of the two layers. Thus the lower layer COT can be estimated by subtraction:

$\hat{\tau}_{lower} = \tau_{\sin gle\_layer} - \hat{\tau}$ where a limits check is added $\hat{\tau}_{lower} = \tau_{lower}^{\min}$

Note ii. Extraction of CTP_{lower} and associated error: CTP_{lower} is essentially given by the retrieved TS parameter but this strictly represents the pressure of an opaque cloud. To improve upon this, the derived COT_{lower} is used to define the lower layer infrared transmission and thus enable the height to be corrected to that of the transmitting lower cloud:

a. For the transmission correction the lower layer COT is limited to be larger than a threshold value $\hat{\tau}_{lower} \geq \tau_{lower\_corr}^{\min}$

b. Infrared transmission and emissivity of lower cloud are calculated $\Gamma_{lower}^{IR} = e^{-\hat{\tau}_{lower}\sec(\zeta_{sat})/2}$ and $\varepsilon_{lower} = 1 - \Gamma_{lower}^{IR}$

c. The opacity corrected radiance (using 10.8 μm) of the lower cloud is then $\hat{L}_{lower}^{10.8} = \dfrac{\left[B^{10.8}\left(\hat{T}_s\right) - B^{10.8}\left(\hat{T}_{fcst}^{skin}\right)\Gamma_{lower}^{IR}\right]}{\varepsilon_{lower}}$ and the equivalent opacity corrected brightness temperature $BT_{lower}^{10.8} = B^{10.8^{-1}}\left(\hat{L}_{lower}^{10.8}\right)$

d. $BT_{lower}^{10.8}$ is now interpreted as a lower CTP by reference to the forecast temperature profile using a reference temperature and pressure, T_{ref} and P_{ref}, and local lapse rate $\lambda_{ref} = \Delta T / \Delta P$. The origin of T_{ref}, P_{ref} *and* λ_{ref} depend on whether a boundary layer inversion is present or not.

   i. Boundary present (INV_BL true):

      1. IF $BT_{lower}^{10.8} > T_{fcst}(P_{fcst}^{Inv\_top})$ then cloud lies <u>within</u> the boundary layer.

         $T_{ref} = T_{fcst}(nlev)$ and $P_{ref} = P_{fcst}(nlev)$ and $\lambda_{ref} = BL_{lapserate}$

      2. IF $BT_{lower}^{10.8} \leq T_{fcst}(P_{fcst}^{Inv\_top})$ then cloud lies <u>above</u> the boundary layer. $T_{ref} = T_{fcst}(P_{fcst}^{Inv\_top})$ and $P_{ref} = P_{fcst}^{Inv\_top}$ and $\lambda_{ref} = \dfrac{\left[T_{fcst}(P_{fcst}^{Inv\_top-1}) - T(P_{fcst}^{Inv\_top-2})\right]}{P_{fcst}^{Inv\_top-1} - P_{fcst}^{Inv\_top-2}}$

   ii. No Boundary layer (INV_BL false):

   $T_{ref} = T_{fcst}(P_{fcst}^{p\_extrap\_high})$ and $P_{ref} = P_{fcst}^{p\_extrap\_high}$ and $\lambda_{ref} = \dfrac{\left[T_{fcst}(P_{fcst}^{p\_extrap\_high}) - T(P_{fcst}^{p\_extrap\_low})\right]}{P_{fcst}^{p\_extrap\_high} - P_{fcst}^{p\_extrap\_low}}$

The lower layer CTP is then calculated from $CTP_{lower} = P_{ref} - \frac{T_{ref} - BT_{lower}^{10.8}}{\lambda_{ref}}$ and the associated error from $\sqrt{S_{CTPlower}} = \frac{\sqrt{S_{\hat{x}}(l,l)}}{\lambda_{ref}}$ where l is the index of the state parameter TS in x.

11 APPENDIX: GRADIENT MODEL WORKINGS

a) Solar overcast reflectance gradient to cloud parameters where:

$$\rho_{\bullet} = \rho_{BD}\mathsf{T}_{2ac} + S \qquad \text{and} \qquad S = \frac{\mathsf{T}_B\mathsf{T}_D\rho_s\mathsf{T}_{2sfc}}{(1-\rho_s\rho_D)};$$

$$\rho'_{\bullet} = \rho'_{BD}\mathsf{T}_{ac} + S'$$

and

$$S' = \frac{(1-\rho_s\rho_D)\left[\mathsf{T}'_D\mathsf{T}_B + \mathsf{T}'_D\mathsf{T}_B\right]\rho_s\mathsf{T}_{sfc} + \mathsf{T}_B\mathsf{T}_D\rho_s^2\mathsf{T}_{2sfc}\rho'_D}{(1-\rho_s\rho_D)^2}$$

$$= \frac{\left[\mathsf{T}'_D\mathsf{T}_B + \mathsf{T}'_D\mathsf{T}_B\right]\rho_s\mathsf{T}_{2sfc}}{(1-\rho_s\rho_D)} + \frac{\mathsf{T}_B\mathsf{T}_D\rho_s^2\mathsf{T}_{2sfc}\rho'_D}{(1-\rho_s\rho_D)^2}$$

$$= S\frac{\left[\mathsf{T}'_D\mathsf{T}_B + \mathsf{T}'_D\mathsf{T}_B\right]}{\mathsf{T}_B\mathsf{T}_D} + S\frac{\rho_s\rho'_D}{(1-\rho_s\rho_D)}$$

b) Solar overcast reflectance gradient to surface reflectance:

$$\frac{\partial\rho_{\bullet}}{\partial\rho_s} = \frac{\partial S}{\partial\rho_s} = \frac{(1-\rho_s\rho_D)\mathsf{T}_B\mathsf{T}_D\mathsf{T}_{2sfc} + \mathsf{T}_B\mathsf{T}_D\rho_s\mathsf{T}_{2sfc}\rho_D}{(1-\rho_s\rho_D)^2}$$

$$= \frac{S}{\rho_s} + \frac{S\rho_D}{(1-\rho_s\rho_D)}$$

12 GLOSSARY

Symbol		Meaning	Units[29]
Text	Maths		
	$\mathbf{x}$	Vector representing state (cloud property) variables	
	$\mathbf{y}$	Vector representing measurements	
	$\mathbf{b}$	Vector representing model parameters	
	$\mathbf{K}_{var}$	Matrix, derivative of *y w.r.t. var*	
	J	Cost	
	J_m	Measurement cost	
	J_a	*a priori* cost	-
	$\mathbf{S}_x$	error covariance of *a priori* information	-
	$\mathbf{S}_b$	error covariance of model parameters	-
	$\mathbf{S}_y$	error covariance of measurements	
	$\mathbf{S}_M$	Solution error covariance arising from measurement error	
	$\mathbf{S}_B$	Solution error covariance from model parameter error	
	$\mathbf{S}_N$	'Null-space' solution error covariance	
	$\mathbf{S}_T$	Total solution error covariance	
	$\mathbf{I}$	Unit matrix	
	α	Marquardt scheme tuning parameter	
COT	τ	Cloud optical thickness referenced to 0.55 μm	-
CRE	r_e	Cloud particle effective radius	μm
CTP	p_c	Cloud top pressure	hPa
CFR	f	Fractional cloud cover (pixel)	-
CPHS		Cloud phase (liquid / solid)	-
TS	T_s	Skin temperature	K
CTH		Cloud top height	m
CTT	T_c	Cloud top temperature	K
	F_{sun}	Solar constant (channel integrated)	W/m^2
	L	Radiance	$mW/ m^2/st/cm$
	$L_\circ$	Clear radiance	$mW/ m^2/st/cm$
	$L_\bullet$	Overcast radiance	$mW/ m^2/st/cm$
	ρ	Reflectance	$mW/ m^2/st/cm$
	$\rho_\circ$	Clear reflectance	$mW/ m^2/st/cm$
	$\rho_\bullet$	Overcast reflectance	$mW/ m^2/st/cm$
	L_{ac}	IR Radiance from atmosphere above cloud	$mW/ m^2/st/cm$
	L_{bc}	IR Radiance upwelling at level	$mW/ m^2/st/cm$
	$L_{ac}^{\downarrow}$	IR Radiance down-welling at level	$mW/ m^2/st/cm$
	B	Planck black body function	$mW/ m^2/st/cm$
	T_{2ac}	Two-path transmittance above cloud (solar)	-
	T_{2sfc}	Two-path transmittance from surface (solar)	-
	T_{ac}	one path transmittance above cloud	-

[29] Units are not given where a mix of variables is implied, e.g. the state vector.

	T_{sfc}	one path transmittance from surface	-
	ρ_s	Surface reflectance	-
	ρ_{BD}	Bi-directional reflectance (of cloud, solar)	-
	ρ_D	Diffuse reflectance	-
	ρ_{FD}	Hemispheric integral of diffuse reflectance	-
	T_B	Beam transmission direct (solar)	-
	T_{FBD}	Hemispheric integral of diffuse beam transmission	-
	T_D	Diffuse transmission	-
	ε	Emissivity, subscript c – cloud, s – surface.	-
	ζ_{sun}	Solar zenith angle	deg
	ζ_{sat}	Satellite (view) zenith angle	deg
	ψ	Relative azimuth between sun and satellite	deg

13 CONSTANTS

Constant	Meaning	Value or source[30]
$x_k^{lower\_\lim}$, $x_k^{upper\_\lim}$	Lower / upper permitted limit to parameter vale	LUT header / etc.. tbc
ΔJ^{thresh}	Cost threshold to determine convergence	1.0
ΔJ_{meas_IR}	IR-based measurement cost threshold for multi-layer cloud detection	25 (currently tuned to SEVIRI); (NB different values for dust, ash and ice/water, TBD)
Cloud Model Parameter Constants for Single layer application		
TS_{Sx}^{SL}	A priori error for Skin Temperature variable; (ocean, land)	1.0, 5.0
COT_{AP}^{SL}	A priori COT; (water, ice)	$10^{1.2}$, $10^{1.2}$
COT_{Sx}^{SL}	A priori error COT	1e8
CTP_{AP}^{SL}	A priori CTP; (water, ice)	850, 400
CTP_{Sx}^{SL}	A priori error CTP	1e6
CRE_{AP}^{SL}	A priori CRE; (water, ice)	8.0, 60.0
CRE_{Sx}^{SL}	A priori error CRE	1e8
CFR_{FG}^{SL}	First Guess CFR	1.0
CFR_{AP}^{SL}	A priori CFR	1.0
CFR_{Sx}^{SL}	A priori error CFR	tiny
Cloud Model Parameter Constants for 2-layer application		
COT_{FG}^{2L}	First guess value for ice layer	0.5
COT_{AP}^{2L}	A priori value for ice layer	0.5
COT_{Sx}^{2L}	A priori error value for ice layer	0.3
ΔP_{FG}^{2L}	Increment of pressure below the tropopause for first guess CTP	100.
P_{fcst}^{2L-wat}	First guess pressure of lower layer in 2-Layer model (target pressure – nearest forecast level used)	800.
CTS_{Sx}^{2L}	A priori error for Skin Temperature variable (proxy lower cloud temperature) in 2-Layer model)	20.
CTP_{Sx}^{2L}	A priori error for CTP in 2-Layer model	100.
CRE_{FG}^{2L}	First Guess CRE in 2-Layer model	15.0
CRE_{AP}^{2L}	A priori CRE in 2-Layer model	15.0

[30] An indicative value is given here but all constants will derive from Static Application Data files.

CRE_{Sx}^{2L}	A priori error CRE in 2-Layer model	5.0
CFR_{FG}^{2L}	First Guess CFR in 2-Layer model	1.0
CFR_{AP}^{2L}	A priori CFR in 2-Layer model	1.0
CFR_{Sx}^{2L}	A priori error CFR in 2-Layer model	tiny
f_o^i	Solar constant for reflectance channels	SAD
$NeBT^i$	Instrument Noise equivalent radiance for thermal channels	SAD
$NeHom^i$	Homogeneity (cloud) Noise equivalent reflectance error (solar channels) or Brightness Temperature error (thermal channels	SAD
$NeCor^i$	Co-registration Noise equivalent reflectance error (solar channels) or Brightness Temperature error (thermal channels	SAD
MQ_{start}	Starting value for LM algorithm α factor	0.01
α_{step}	Step factor for LM algorithm	10.
$P_{fcst}^{search\_top}$	Lowest pressure to be used in search for boundary layer inversion top (target pressure – nearest forecast level used)	700.
$\Delta P_{overshoot}$	Permitted tropopause overshooting delta pressure	80.
σ_{TS}	Permitted number of standard deviations from forecast skin temperature	3.0
$\Delta T_{lower-upper}$	Lower limit on difference between upper and lower cloud temperatures in 2L operation	10.
$\tau_{lower}^{\min}$	Lower limit on lower layer COT	0.05
$\tau_{lower\_corr}^{\min}$	Lower limit on lower layer COT for transmission correction	1.0
$P_{fcst}^{p\_extrap\_high}$	High pressure level for lower layer cloud CTP interpolation (target pressure – nearest forecast level used)	880
$P_{fcst}^{p\_extrap\_low}$	High pressure level for lower layer cloud CTP interpolation (target pressure – nearest forecast level used)	700